i-bodies, Human Single Domain Antibodies That Antagonize Chemokine Receptor CXCR4*[S]

Katherine Griffiths,[a] Olan Dolezal,[b] Benjamin Cao,[c,d] Susan K. Nilsson,[c,d] Heng B. See,[e,f] Kevin D. G. Pfleger,[e,f,g] Michael Roche,[h,i] Paul R. Gorry,[j] Andrew Pow,[a1] Katerina Viduka,[a2] Kevin Lim,[a3] Bernadine G. C. Lu,[a4] Denison H. C. Chang,[a5] Thomas Murray-Rust,[a] Marc Kvansakul,[k] Matthew A. Perugini,[k] Con Dogovski,[k6] Marcel Doerflinger,[a7] Yuan Zhang,[l] Kathy Parisi,[a,k] Joanne L. Casey,[a7] Stewart D. Nuttall,[b] and Michael Foley[a,k8]

From [a]AdAlta Pty. Ltd., 15/2 Park Dr., Bundoora, Victoria 3083, [b]Biomedical Manufacturing, CSIRO Manufacturing, 343 Royal Parade, Parkville, Victoria 3052, the [c]Australian Regenerative Medicine Institute, Monash University, Wellington Road, Clayton, Victoria 3800, [d]Biomedical Manufacturing, CSIRO Manufacturing, Bayview Avenue, Clayton, Victoria 3168, the [e]Harry Perkins Institute of Medical Research, Nedlands, Western Australia 6009, the [f]Centre for Medical Research, University of Western Australia, Crawley, Western Australia 6009, [g]Dimerix Bioscience Ltd., Nedlands, Western Australia 6009, the [h]Doherty Institute for Infection and Immunity, University of Melbourne, 792 Elizabeth Street, Melbourne, Victoria 3000, the [i]Burnet Institute, 85 Commercial Road, Melbourne, Victoria 3004, the [j]School of Health and Biomedical Sciences, College of Science, Engineering and Health, RMIT University, Melbourne, Victoria 3001, the [k]Department of Biochemistry and Genetics, La Trobe Institute for Molecular Science, La Trobe University, Melbourne, Victoria 3086, and the [l]Department of Medicine, St. Vincent's Hospital, University of Melbourne, Fitzroy, Victoria 3065, Australia

CXCR4 is a G protein-coupled receptor with excellent potential as a therapeutic target for a range of clinical conditions, including stem cell mobilization, cancer prognosis and treatment, fibrosis therapy, and HIV infection. We report here the development of a fully human single-domain antibody-like scaffold termed an "i-body," the engineering of which produces an i-body library possessing a long complementarity determining region binding loop, and the isolation and characterization of a panel of i-bodies with activity against human CXCR4. The CXCR4-specific i-bodies show antagonistic activity in a range of *in vitro* and *in vivo* assays, including inhibition of HIV infection, cell migration, and leukocyte recruitment but, importantly, not the mobilization of hematopoietic stem cells. Epitope mapping of the three CXCR4 i-bodies AM3-114, AM4-272, and AM3-523 revealed binding deep in the binding pocket of the receptor.

Single domain antibodies and alternative scaffolds have been promoted as attractive next-generation antibodies with the potential to address some of the limitations of monoclonal antibodies (1–4). Indeed several have been reported in recent years that target antigens that are refractory to traditional antibody therapies, such as G protein-coupled receptors (GPCRs)[9] (5, 6). The variable new antigen receptors (V_{NAR}s) from sharks are single-domain antibody-like molecules that have been reported to have exquisite stability (7, 8) and the ability to bind with high affinity and specificity to target molecules (9–11). The observation by Streltsov *et al.* (12) that the V_{NAR} was structurally similar to the i-set family of immunoglobulin domains (Igs) suggested that these are suitable scaffolds to engineer into a human equivalent of the V_{NAR}. To this end, we have engineered a human "i-body" scaffold from an Ig domain of human neural cell adhesion molecule 1 (NCAM) by incorporating two binding regions into this protein, thus combining complementarity determining-like binding regions (CDRs) with the innate stability properties of a human Ig domain.

The chemokine receptor CXCR4 is a member of the CXC chemokine receptor family of GPCRs, and together with its ligand CXCL12 (also known as stromal cell-derived factor 1, SDF-1), they are important therapeutic targets. CXCR4 has

[1] Present address: Compugen Ltd., 260 East Grand Ave., South San Francisco, CA 94080.
[2] Present address: Dept. of Economic Development, Jobs, Transport and Resources, AgriBio Centre, 5 Ring Rd., Bundoora, Victoria 3083, Australia.
[3] Present address: Imunexus, 343 Royal Parade, Parkville, Victoria 3052, Australia.
[4] Present address: CSL Ltd., 45 Poplar Rd., Parkville, Victoria 3052, Australia.
[5] Present address: Virbac, Milperra, New South Wales 2214, Australia.
[6] Present address: Dept. of Biochemistry and Molecular Biology, Bio21 Molecular Science and Biotechnology Institute, University of Melbourne, Melbourne, Victoria 3010, Australia.
[7] Present address: Nexvet, 21-31 Wright St., Clayton, Victoria 3168, Australia.
[8] To whom correspondence should be addressed: Dept. of Biochemistry, La Trobe University, Plenty Road, Bundoora, Victoria 3086, Australia. E-mail: m.foley@latrobe.edu.au.

[9] The abbreviations used are: GPCR, G protein-coupled receptor; V_{NAR}, variable new antigen receptor; NCAM, neural cell adhesion molecule 1; CDR, complementarity determining region; PDB, Protein Data Bank; RLU, relative light unit; SPR, surface plasmon resonance; hu, human; mu, murine; BM, bone marrow; PB, peripheral blood; CB, cord blood; HSC, hematopoietic stem cell; Env, envelope; ECL, extracellular loop; HBSS, Hanks' balanced salt solution; PE, phycoerythrin; BRET, bioluminescence resonance energy transfer.

been shown to be up-regulated in a number of cancers (13), plays an important role in the maintenance of stem cells in the bone marrow (14), serves as a co-receptor for HIV (15), and more recently has been demonstrated to be a central player in the development of fibrosis (16–18). The only approved inhibitor of CXCR4 is the small molecule AMD3100 (plerixafor), for application in mobilization of hematopoietic stem cells (19). Additional CXCR4 inhibitors that have been well described in the literature include the small molecule MSX-122 (20) and peptide BL-8040 (21). Nanobodies (6) and various other peptides, small molecules, and antibodies (22, 23) have also been described (24).

We describe here the engineering of an i-body library from a human single Ig domain and the generation of specific high affinity binders to CXCR4 that appear to be blocking signaling from this GPCR in a selective fashion. Moreover, we demonstrate that these i-bodies can penetrate deep into the ligand binding pocket and contact residues that were previously only accessible to small molecule drugs. Finally, we show that the i-bodies can block inflammatory cell migration but do not mobilize stem cells, a valuable asset for long term therapy for cancer and fibrosis.

Experimental Procedures

Molecular Biology and Protein Purification

Restriction enzymes and ligase were from New England Biolabs or Promega. PCR was performed using AmpliTaq Gold® (Life Technologies, Inc.) or *Vent* DNA polymerase (New England Biolabs). Genes were expressed from vector pGC (25) using TG1 *Escherichia coli* cells (Lucigen) into the periplasmic space, then isolated using the method of Minsky *et al.* (26), and purified by immobilized metal affinity chromatography (His60 Nickel Superflow Resin, Clontech) or affinity chromatography (anti-FLAG M2 affinity gel, Sigma), followed by ion exchange (HiTrap Q FF, GE Healthcare) or gel filtration (Superdex 200 or Superdex 75, GE Healthcare). Proteins were C-terminally tagged with His_6, FLAG peptide, or Im7 (27) combined with -FLAG-His_6. The M13 bacteriophage vector pHENH6 (gift from H. Hoogenboom) (28) and TG1 *E. coli* cells were used for production of phage particles. The coding sequence for the wild-type human NCAM Ig domain 1 was amplified from a Human Leukocyte Large-Insert cDNA library (BD Biosciences and Clontech) using oligonucleotides A0657 (5′-gtctcgcgc-cccagccggccatggccctgcaggtggatattgttcccagccag-3′) and A0658 (5′-gctggttgcggccgcctgaaagatcttcacgttgacggtggc-3′) and designated as clone 21H-5 (exact match to residues 20–115 from existing GenBank™ accession number AAH29119.1, residues 20–115).

Crystallization and Structure Determination

Crystallization trials for 21H-5 were set up using protein concentrated to 30 mg/ml using centrifugal concentrators (Millipore). Crystals were grown by the sitting drop method at room temperature in 1.45 M tri-sodium citrate, pH 6.88. The crystals belong to space group $P2_1$ with $a = 23.85$ Å, $b = 107.327$ Å, $c = 41.748$ Å and $\alpha = 90°$, $\beta = 99.573°$, $\gamma = 90°$. The asymmetric unit contains two 21H-5 chains and has 38% solvent content. Diffraction data were collected from crystals flash-cooled in mother liquor supplemented with 30% ethylene glycol at 100 K using beamline MX2 at the Australian Synchrotron. Diffraction data were processed with XDS (29), and programs of the CCP4 suite and all complex structures were solved by molecular replacement with PHASER (30) using the structure of rat NCAM-1 (PDB 1QZ1) as a search model. The final models were built with Coot (31) and refined with Phenix (32). All data collection and refinement statistics are summarized in supplemental Fig. 1. All software was accessed via SBGrid (33). Figures were prepared using PyMOL (The PyMOL Molecular Graphics System, Version 1.7.4 Schrödinger, LLC).

i-Body Engineering

23B-2 was engineered by replacing the 21H-5 residues [82]EDGS[85] with the V_{NAR} clone 1A-7 residues [88]SDAMSNYSY-PIS[99] (34) using a splice-overlap PCR method (International Patent AU2005/000789; WO/2005/118629). The 15-mer i-body library was constructed by site-directed mutagenesis (35) and cloned into pHENH6. The i-body 10–20 library was based on the parent clone 21H-5 and was synthesized by GeneArt (now Life Technologies, Inc.) using synthetic oligonucleotides to produce insert sizes in the range 324–354 bp. Fully randomized 6-residue CDR1 and 10–20-residue CDR3 loop regions replaced NH_2-[27]DAKDKD[32]-COOH and NH_2-[80]TGEDGSES[87]-COOH, respectively, from 21H-5. These randomized regions were synthesized with nucleotide mixtures of N nucleotide ambiguity at the first and second bases of the codon (25% cytosine, 25% thymine, 25% adenine, 25% guanine) and K nucleotide ambiguity at the third base of the codon position (50% guanine and 50% thymine). The library was amplified and cloned into pHENH6 via SfiI and NotI cloning sites (thus fusing the i-body proteins with the bacteriophage pIII coat protein), and transformed into TG1 cells.

Antigens

Monoclonal antibody 5G8, which recognizes *Plasmodium falciparum* apical membrane antigen 1 (3D7 strain) (28), was immobilized on Nunc Maxisorp Microplates (Thermo Scientific) at 1 μg/ml. Integral Molecular provided the lipoparticles (in biotinylated and non-biotinylated formats) harboring the human CXCR4 protein, and "null" lipoparticles lacking it. Streptavidin-coated M280 Dynabeads were from Invitrogen.

Phage Affinity Panning

The 15-mer and i-body 10–20 libraries (in pHENH6 and TG1 cells) were amplified at the beginning of each panning campaign according to the following procedure: 1 ml of library stock was inoculated into 10 ml of 2YT medium and incubated for 1 h at 37 °C with shaking. Ampicillin (Sigma) was added to a final concentration of 50 μg/ml, and after 1 h of incubation at 37 °C the culture was inoculated into 200 ml of 2YT containing 100 μg/ml ampicillin, 1% (w/v) glucose (Sigma) and incubation was continued at 37 °C with shaking until the absorbance at $A_{600\,nm}$ was 0.4–0.6. A 25-ml aliquot was removed, to which 10^{11}–10^{12} of kanamycin-resistant M13KO7 helper phage particles (New England Biolabs) were added. The culture was incubated for 1 h without shaking at 37 °C, and then the cell pellet was collected by centrifugation at 8,000 × *g*, resuspended in 3

ml of 2YT, and inoculated into 200 ml of 2YT containing 100 μg/ml ampicillin and 70 μg/ml kanamycin (Sigma). The culture was incubated for 15 h with shaking at 30 °C. The supernatant was clarified twice by centrifugation at 10,000 $\times$ g for 10 min, and 0.2 volumes of 20% (w/v) PEG 8000 (Sigma) and 2.5 M NaCl (Sigma) was added. The phage particles were precipitated by incubation on ice for 2 h with gentle agitation, then collected by centrifugation at 10,000 $\times$ g for 30 min, and resuspended in 2 ml of PBS. To remove unwanted phage binders to the milk powder blocking solution used in subsequent steps, 500 μl of phage preparation solution was combined with 500 μl of 10% (w/v) milk powder in 1$\times$ PBS.

Dynabeads (50 μl) were washed twice with 1 ml of PBS and then resuspended in 1 ml of 5% (w/v) milk powder in 1$\times$ PBS (MPBS) and incubated at room temperature for 60 min with very gentle rotation. The blocking solution was removed, and beads were resuspended in 50 μl of MPBS. Solution-based panning was then performed using two preliminary negative selection approaches (depletion and competition) to minimize the recovery of unwanted binders (*i.e.* binders to the blocking solution, Dynabeads, or lipoparticle scaffold). In the depletion-style negative selection method, binders to biotinylated null lipoparticles were removed prior to panning on CXCR4 lipoparticles as follows: 40 μl of biotinylated null lipoparticles were combined with 1 ml of phage and incubated for 30 min at room temperature with mixing. Blocked streptavidin beads (50 μl) were then added and incubated for 30 min at room temperature with mixing. Magnetic beads along with biotinylated null lipoparticles and bound phage were removed using a magnetic rack, and the remaining phage supernatant was used for panning against CXCR4 lipoparticles. In the competition-style negative selection method, non-biotinylated null lipoparticles were present in the panning solution where they "competed" with biotinylated CXCR4 lipoparticles for unwanted nonspecific binders; 40 μl of non-biotinylated null lipoparticles were combined with 1 ml of phage and incubated for 30 min at room temperature with mixing. This mixture was used directly in panning against CXCR4 lipoparticles.

For panning, 50 μl of biotinylated CXCR4 lipoparticles (equivalent to 40 units of CXCR4) were combined with negatively selected phage and incubated at room temperature for 2 h with mixing. 50 μl of blocked Dynabeads were added, and incubation was continued for 30 min at room temperature with mixing, before magnetic capture of the assembled beads, lipoparticles, and bound phage. Unbound phage were removed by washing with PBS and PBS + 0.5% (v/v) Tween (PBS-T) as follows: round one (R1), three washes with PBS; R2 three washes with PBS-T and then three washes with PBS; R3 and R4, six washes with PBS-T and then six washes with PBS for rounds three and four, and except for R4 the final wash solution was incubated for 5 min prior to removal. Following the last wash of each round, beads were transferred to a clean tube, and antigen-bound phage was eluted with 500 μl of 0.1 M glycine (pH 2.0). The eluate was neutralized to pH 8 with 1.5 M Tris-HCl and used to infect TG1 cells to amplify the selected i-body clones for the subsequent panning round. Amplification of eluted phage between each panning round was performed as follows: eluted phage were added to 10 ml of TG1 cells in log phase, incubated at 37 °C for 30 min without agitation, and then for 30 min with agitation. 10^{11}–10^{12} of M13KO7 helper phage particles were added to the infected cells, and incubation at 37 °C was continued for 30 min without shaking. The culture was then inoculated into 200 ml of 2YT containing ampicillin at 100 μg/ml and kanamycin at 70 μg/ml and incubated overnight at 30 °C with shaking. Phage were precipitated as described above and subjected to the next panning round. Phage were titered in between panning rounds as follows: 10 μl of each phage preparation was added to 490 μl of log-phage TG1 cells; 20 μl was then removed and diluted with 2YT in a 10-fold series in a 96-well plate. 20 μl of each dilution point was spread onto an agar plate containing ampicillin and incubated overnight at 37 °C.

ELISAs

Phage ELISAs were performed with pools of phage particles eluted from panning rounds and with single-clone phage particles. To prepare phage particles from an individual clone, 10 ml of 2YT with 100 μg/ml ampicillin was inoculated with a single colony and incubated with shaking at 37 °C for 4 h. Helper phage and kanamycin were added, and the cultures were incubated for 15 h as described above. Phage particles were precipitated and resuspended as described above except that the final resuspension volume was 1 ml. For ELISAs, the wells of 96-well plates (Nunc) were coated in duplicate with 100 μl per well of mAb 5G8 or lysozyme at 1 μg/ml or with lipoparticles (CXCR4, CCR5, or null) at 1 unit/well. Phage were diluted at least 1:10 in probing solution (5% MPBS, to normalize titers), added to the wells, and incubated for 60 min at room temperature. The wells were washed five times with PBS-T, and then bound phage were detected with an anti-M13-HRP antibody (GE Healthcare) by using 3,3′,5,5′-tetramethylbenzidine (Thermo Fisher) as an enzyme substrate.

Thermal and pH Stability

Separate 4-μl aliquots of crude periplasmic extracts of i-body AD5G8-5 were incubated for 30 min at room temperature, 30, 40, 50, 60, 70, 80, 90, or 99 °C, and then cooled at 4 °C for 30 min. Samples were centrifuged to collect precipitated protein, and the remaining soluble protein was analyzed by SDS-PAGE and visualized with Coomassie staining.

For the long term stability trial, separate 50-μl aliquots (in singlicate) of AD5G8-5 at 0.12 mg/ml were adjusted to pH values of 3, 4.5 (using 0.2 M Na$_2$HPO$_4$ and 0.1 M citric acid), and 7.4 (using PBS), and pH values of 8.5 and 11.0 (using 25 mM borax buffer) and incubated at 4, 37, and 50 °C for 4 weeks. Unheated control samples were stored at −20 °C throughout. Following incubation, samples were neutralized to pH 7.4 with 1 M Tris, pH 11.5 (for samples at pH 3.0 and 4.5), or with 1 M HCl (for samples at pH 8.5 and 11.0). Residual active protein was quantified by fully automated SPR-based concentration assay described previously (7). Residual binding activity in diversely treated anti-5G8 i-body samples was determined using a ProteOn XPR36 instrument (Bio-Rad). All immobilization and concentration determination measurements were performed at 25 °C with instrumental fluidics primed in 1$\times$ HBS-EP + (10 mM HEPES, 150 mM NaCl, 3 mM EDTA 0.05% (v/v) surfactant P20, pH 7.4). The concentration detection method was config-

ured as a direct detection assay with quantification estimates being derived from a calibration standard, that being an untreated sample stored at 4 °C ($t = 0$). Standard curve was established by a parallel injection of six different concentrations of $t = 0$ sample (500, 1,000, 2,000, 4,000, and 8,000 ng/ml) across the immobilized 5G8 IgG protein. Residual active concentrations of unknown samples were determined by injecting six samples simultaneously at 25 ml/min for 60 s and comparing their initial binding rates (at $t = 5$–20 s) to those generated by the calibration standards. Bound samples were regenerated from the surface with a single injection of 10 mM glycine, pH 2.2, at 100 ml/min for 15 s.

SPR Experiments

Kinetic binding analysis of selected i-bodies with immobilized CXCR4 lipoparticles was performed at 25 °C using BIAcore T200 instrument (GE Healthcare, Uppsala, Sweden). Streptavidin immobilization was performed in 1× HBS-P+ running buffer (10 mM HEPES, 150 mM NaCl, 0.05% (v/v), Tween 20). Amine coupling kit (GE Healthcare) and the instructions therein were utilized for the attachment of streptavidin (Sigma; diluted to 100 μg/ml in 10 mM sodium acetate buffer, pH 4.5) in all four channels on the sensor chip surface simultaneously, resulting in >6,000 response units of streptavidin being coupled (1 response unit = 1 pg of protein/mm²). All binding experiments involving lipoparticles were performed with 1× HBS/BSA (10 mM HEPES, 150 mM NaCl, 1 mg/ml BSA) as instrument running buffer. Biotinylated CXCR4 lipoparticles (Integral Molecular, catalog no. LEV-101B; 3.6 units/ml) were typically diluted 1:20 in the running buffer and immobilized onto a streptavidin-containing channel by injecting at 2 μl/ml for 1,800 s resulting in captured response levels of greater than 2,500 response units. Biotinylated CCR5 and null lipoparticles, used as off-target controls, were immobilized in a similar manner. To determine binding kinetics, serial dilutions (3-fold) of i-bodies diluted in 1× HBS/BSA were injected over immobilized lipoparticles with the association and dissociation phases monitored for 60 and 600 s, respectively. A control measurement of the instrument running buffer ("zero-buffer" blank) solution was also included for double referencing purposes. No regeneration of CXCR4 lipoparticle surface was required between injection cycles as bound i-bodies fully dissociated within 600 s in the running buffer.

An SPR assay was designed to assess competition between CXCL12 and the i-bodies. This consisted of i-body injection followed by CXCL12 injection. A streptavidin chip containing immobilized biotinylated CXCR4 lipoparticles was prepared as described above. The assay assumes that binding competition occurs when the pre-bound i-body on the CXCR4 surface, at least partially, reduces the CXCL12 binding response. Injection of running buffer (RB) prior to CXCL12 ligand injection provided a baseline (no inhibition) response.

Circular Dichroism Spectroscopy

CD spectra were recorded using an AVIV Model 420 CD spectrometer using similar methods described previously (36). Protein (0.15 mg/ml in PBS) was subjected to wavelength scans spanning 190–250 nm at 20 and 80 °C, using a step size of 0.5 nm with a 3-s averaging time in a 1-mm stoppered quartz cuvette.

Analytical Ultracentrifugation

Sedimentation velocity experiments were conducted in a Beckman model XL-A analytical ultracentrifuge at a temperature of 20 °C using a similar method reported previously (37). Briefly, 380 μl of sample (0.15 mg/ml) and 400 μl of reference solution (10 mM phosphate, 137 mM NaCl, pH 7.4) were loaded into a conventional double sector quartz cell and mounted in a Beckman 4-hole An-60 Ti rotor. Samples were centrifuged at a rotor speed of 40,000 rpm, and the data were collected at 5-min intervals and a single wavelength (280 nm), using a step-size of 0.003 cm without averaging. Solvent density (1.005 g/ml at 20 °C) and viscosity (1.018 centipoise), as well as estimates of the partial specific volume (21H5-FF, 0.718 ml/g at 20 °C; AD5G8-5-FF, 0.720 ml/g at 20 °C) and hydration estimate (21H5-FF, 0.460 g/g; nd AD5G8-5-FF, 0.449) were computed using the program SEDNTERP (38). Sedimentation velocity data at multiple time points were fitted to continuous size distribution models (39) using the program SEDFIT.

In Vitro Cell Binding Assays

Namalwa, NCI-H69, Jurkat, CCRF-CEM, Ramos, HL-60, A498, MOLP-8, and MOLT-4 cell lines were cultured in RPMI 1640 medium supplemented with 10% fetal bovine serum (Gibco) in an atmosphere of 5% CO_2 and 95% humidity at 37 °C. A short tandem repeat assay to detect 20 loci was used to confirm cell identity. A Mycoalert kit (Lonza) was used to monitor for mycoplasma contamination. Following growth to 60–80% confluence, cells were harvested in 15-ml centrifuge tubes, passed through a cell strainer, resuspended in growth medium, and counted. Cells were transferred to 96-well tissue culture plates (Costar) (2×10^5 cells/well) and centrifuged at $1,000 \times g$ at 4 °C for 5 min, and the medium was removed by aspiration. The cells were resuspended in 100 μl of PBS containing CXCR4-specific mAb 12G5 (catalog no. MAB170, R&D Sytems) or isotype control antibody mIgG2a (catalog no. 7076s, Cell Signaling Technology) and then incubated at 4 °C for 45 min. The cells were washed twice with 300 μl of ice-cold PBS and resuspended in 100 μl of PBS containing PE goat anti-mouse IgG secondary antibody (catalog no. 405307, Bio-Legend) and incubated at 4 °C for 40 min in the dark. The cells were washed twice with 300 μl of ice-cold FACS buffer (PBS + 2% (v/v) fetal bovine serum), centrifuged at 1,000 rpm for 5 min, resuspended in 300 μl of ice-cold FACS buffer, and analyzed by fluorescence using a FACSCalibur instrument (BD Biosciences). Cells staining positive for 12G5 were gated, and of these cells the percentages of 12G5 and isotype control mIgG2a staining were determined.

To examine the binding of i-bodies to the above cancer cell lines, cultured cells in 96-well tissue culture plates (2×10^5 cells/well) were centrifuged at 1,000 rpm at 4 °C for 5 min and resuspended in 100 μl of PBS buffer containing i-bodies at various concentrations. Namalwa cells were treated with i-bodies or mAb 12G5 (R&D Systems) at 10, 4.7, 2.1, 1, 0.47, 0.21, 0.1, 0.01, and 0.001 μM, whereas NCI-H69, Jurkat, CCRF-CEM, Ramos, HL-60, A498, MOLP-8, and MOLT-4 cells were treated

with i-bodies at 10, 1, and 0.001 μM. Following incubation at 4 °C for 60 min, cells were washed twice with 300 μl of ice-cold FACS buffer and then resuspended in 100 μl of buffer containing anti-His-PE antibody (catalog no. 130-092-691, Miltenyi Biotec). Washing and FACS analysis were performed as described above.

β-Arrestin Activation

The PathHunter® β-arrestin assay (DiscoveRx) was performed according to the manufacturer's protocol to assess binding of i-bodies to cells expressing various chemokine receptors. The receptors (and corresponding agonists) tested were as follows: CCR1 (CCL3); CCR2 (CCL2); CCR3 (CCL13); CCR4 (CCL22); CCR5 (CCL3); CCR6 (CCL20); CCR7 (CCL19); CCR8 (CCL1); CCR9 (CCL25); CCR10 (CCL27); CX3CR1 (fractalkine); CXCR1 (CXCL8); CXCR2 (CXCL8); CXCR3 (CXCL11); CXCR4 (CXCL12); CXCR5 (CXCL13); CXCR6 (CXCL16); CXCR7 (CXCL12); and CMKLR1 (chemerin). Cells were seeded into white walled 384-well tissue culture-treated microplates (Corning Glass) and normalized at 5,000 cells (or 10,000 cells for CXCR4) in a total volume of 20 μl. Cell growth was at 37 °C (5% CO_2, 95% relative humidity). 5 μl of i-body or AMD3100 (Tocris Bioscience) was then added to singlicate wells. The i-body or AMD3100 concentrations tested were as follows: ADCX99 (2.6 μM); AM1-126 (1.4 μM); AM1-320 (1.6 μM); AM3-114 (0.6 μM); AM4-272 (1.4 μM); AM3-523 (1.0 μM); AM4-746 (2.2 μM); AM4-1121 (1.9 μM); and AMD3100 (0.5 μM). Following incubation of the plates at 37 °C for 30 min, agonists were then added at the EC_{80} concentration and incubation was continued at 37 °C for 90 min (or 180 min for CCR1). Assay signal was generated through a single addition of 15 μl (50% v/v) of PathHunter detection reagent mixture, followed by a 1-h incubation at room temperature. Microplates were read following signal generation with a PerkinElmer Life Sciences Envision instrument for chemiluminescent signal detection of relative light units (RLU). Compound activity was analyzed using the CBIS data analysis suite (ChemInnovation). % inhibition = 100% × (1 −(mean RLU of test sample − mean RLU of vehicle control)/(mean RLU of EC_{80} control − mean RLU of vehicle control)).

BRET β-arrestin assays were carried out as described previously (40). HEK293FT cells were transfected with cDNA using FuGENE 6 (Promega). 5 μM coelenterazine h (Promega) in HBSS was used as the luciferase substrate solution. Data are means ± S.E. of four independent experiments carried out in duplicate. BRET EC_{50} data shown in Table 1 were generated by calculating the EC_{50} of each repeat and then establishing the mean ± S.E. of these values.

cAMP Assay

The HitHunter® cAMP XS+ assay (DiscoveRx, part no. 90-0075) was performed according to the manufacturer's protocol in Gi mode. Cells (CHO-K1) (10,000 cells/well) were seeded in duplicate (in DiscoveRx Assay Complete Cell Plating Reagent 2, part no. 93-0563R2A) in a total volume of 20 μl into white walled 384-well microplates (Corning Glass, part no. 3570) and incubated at 37 °C overnight. Cell growth was at 37 °C and 5% CO_2, 95% relative humidity. Medium was aspi-

rated from the cells and replaced with 10 μl of 1:1 HBSS, 10 mM HEPES/cAMP XS+ antibody reagent (Life Technologies, Inc., catalog no. 14025-076/15630-080). i-bodies (10 μM, 3-fold dilutions, 10-point curve) were pre-incubated with cells for 30 min at 37 °C, followed by the addition of CXCL12 (DiscoveRx part no. 92-1011) at the EC_{80} (3.2 nM) and forskolin at the EC_{80} (15 μM) (Cayman Chemicals, part no. 11018) and incubated for another 30 min at 37 °C. Assay signal was generated through incubation with 20 μl of cAMP XS+ ED/CL lysis mixture for 1 h at room temperature followed by incubation with 20 μl of cAMP XS+ EA reagent for 3 h at room temperature (DiscoveRx, part no. 90-0075). Chemiluminescent signal from microplates was read with a EnVision^{TM} instrument (PerkinElmer Life Sciences). Percent inhibition of cAMP production was calculated using the following formula: % inhibition = 100% × (mean RLU of test sample − mean RLU of EC_{80} control)/(mean RLU of forskolin positive control − mean RLU of EC_{80} control).

Ca²⁺ Assay

A Screen Quest^{TM} Fluo-8 No Wash kit (AAT Bioquest, catalog no. 36315) was used according to the manufacturer's protocol. HEK293T Gαqi5 cells stably expressing human CXCR4 receptor (catalog no. CG1004, Multispan) were cultured in DMEM at 5% CO_2, 95% relative humidity at 37 °C. Cells were seeded in triplicate into a 384-well plate (catalog no. 354663, Corning BioCoat) at 7,000 cells per well in 40 μl and cultured overnight. i-Bodies (8 μM to 0.41 nM) and AMD3100 (10 μM to 0.51 nM) (Tocris) were pre-incubated with cells for 30 min before addition of CXCL12 (PeproTech) at the EC_{80} (77.8 nM). Calcium dye loading buffer (10 μl) was added to the cells and incubated for 1 h at 37 °C. Compounds (i-bodies, AMD3100, and HBSS in agonist mode; CXCL12 EC_{80} and HBSS in antagonist mode) were injected into the wells at the 19th second and calcium flux was monitored for 120 s using a FLIPR 384 instrument (Molecular Devices). EC_{50} ± S.E. (on triplicates) was determined from data normalized against buffer wells set as 100% inhibition and CXCL12 at EC_{80} set as 0% inhibition.

HIV Entry Inhibition Assays

Env-pseudotyped luciferase reporter viruses 1109-F-30, VSVG, and YU-2 were produced and titrated as described previously (41). NP2-CD4/CXCR4 or NP2-CD4/CCR5 cells (1 × 10^4 in 100 μl; a kind gift from N. Shimizu and H. Hoshino) were seeded in Dulbecco's modified Eagle's medium supplemented with 10% (v/v) fetal calf serum, 100 μg/ml penicillin and streptomycin, 500 μg/ml G418, and 1 μg/ml puromycin in flat-bottom 96-well plates (Nunc) and incubated at 37 °C (5% CO_2, 95% relative humidity) for 24 h prior to infection. Medium was aspirated and replaced with 100 μl of medium containing i-bodies (1 μM, 5-fold dilutions, 6-point curve), AMD3100 (2 μM, 5-fold dilutions, 8-point curve), or PBS (5.8%, v/v) for untreated cells and incubated for 30 min at 37 °C. Treated and untreated cells were infected with 200 $TCID_{50}$ of Env-pseudotyped luciferase reporter viruses or mock-infected in 100 μl of medium and incubated for 12 h at 37 °C. The inoculum was removed and replaced with fresh medium containing inhibitor, and the cells were incubated at 37 °C for a total of 72 h. The level of HIV-1 entry was measured by luciferase activity in cell lysates accord-

ing to the manufacturer's protocol (Promega, Luciferase Assay System). Luminescence was measured using a FLUOstar microplate reader (BMG). Background activity was assessed by mock-infected cells and was subtracted from all wells. To calculate the percentage of HIV-1 entry in the presence of antibody, the amount of luciferase in cells treated with an antibody was expressed as a percentage of that in untreated cells. Inhibition assays for 1109-F-30 were performed twice for all i-bodies except AM3-114 and AM4-746, for which assays were performed three times. Inhibition assays for VSVG were performed once with all i-bodies. Inhibition assays for YU-2 were performed once with 21H5, AM3-114, and AM4-746. All assays contained replicates in duplicate. Graphs were derived by combining the mean from each replicate data point (from either 1, 2, or 3 experiments) into one figure. IC_{50} values were derived by fitting a curve to each individual experiment and then obtaining the mean and standard deviation from the combined IC_{50} values.

In Vivo Cell Migration Assay

Following acclimation, 7-week-old BALB/C mice were anesthetized with an isoflurane/O_2 mixture, and 0.2 ml/g initial body weight sterile air was injected under the back skin to create an air pouch. This was repeated on day 3. On day 6, mice were divided into groups (five mice per group) and received an intraperitoneal injection of 0.5 ml of PBS $\pm$ 10 mg/kg of i-bodies or AMD3100 (Sigma). Thirty minutes later, PBS or 2 μg of CXCL12 (Biolegend) was injected into the air pouch. Four hours later, the mice were killed in a CO_2 chamber, and the air pouches were lavaged and washed, and cells were counted following trypan blue staining. All the procedures were conducted in accordance with the Guide for the Care and the Use of Laboratory Animals (National Institutes of Health) and approved by MuriGenics' in-house IACUC.

Epitope Mapping

Epitope mapping of binding of AM3-114, AM3-523, and AM4-272 i-bodies to human CXCR4 was conducted by Integral Molecular using their Shotgun Mutagenesis Mapping Service. HEK293T cells expressing the CXCR4 library of 733 mutants (or an empty-vector control) were cultured in 384-well format, and CXCR4 expression and folding were monitored using an anti-FLAG mAb and an anti-CXCR4 mAb 12G5. Binding by anti-CXCR4 i-bodies using a high throughput immunofluorescence FACS assay was conducted as follows. i-Bodies were added to CXCR4 mutant-expressing cells at 1 μg/ml (AM3-114 and AM3-523) or 2 μg/ml (AM4-272) and incubated for 60 min at room temperature. The anti-His secondary antibody (catalog no. MAB050, R&D Systems) was then added at 1:200 (v/v) followed by 30 min of incubation at room temperature. Finally, the tertiary antibody AlexaFluor® 488-AffiniPure goat anti-mouse IgG (H+L) (catalog no. 115-545-003, Jackson Immuno-Research) was added at 1:400 (v/v) and incubated at room temperature for 30 min. Each raw datum point was background-subtracted (background being the signal obtained for binding to cells transfected with empty vector) and normalized to the value for reactivity with wild-type CXCR4. For each clone, the mean binding values for the anti-CXCR4 i-body were plotted as

a function of its mean CXCR4 expression value. Critical residues for i-body binding were identified as those that were positive for two internal controls as follows: CXCR4 expression using an anti-FLAG mAb (>70% wild type) and correct folding of CXCR4 using anti-CXCR4 mAb 12G5 (>50% wild type). Critical residues were further categorized into primary, secondary, and tertiary. "Primary" critical residues whose side chains make the highest energetic contributions to the interaction between each i-body and the GPCR showed <30% of wild-type CXCR4 reactivity for AM3-114 and AM4-272 or <15% of wild-type CXCR4 reactivity for AM3-523. "Secondary" residues with reactivity values between 30 and 40% were likely to contact i-bodies with lower energy and possibly affect presentation of the epitope. "Tertiary" residues with reactivity values between 40 and 50% appeared to affect the binding of the i-body but with no clear distinction as to how or why.

Cord Blood, Bone Marrow, and Hematopoietic Stem Cell Binding

Umbilical Cord Blood and Human Bone Marrow—Umbilical cord blood (CB) and human bone marrow (BM) were obtained from the Mercy Hospital for Women (East Melbourne, Australia), and patients undergoing hip replacement at St. Vincent's Public Hospital or St. Vincent's Private Hospital (East Melbourne, Australia), respectively, and were collected as described previously (42, 43). The ethics committee of each respective hospital approved all experiments. Enriched human BM CD34$^+$ cells and purified CB CD34$^+$ cells were isolated as described previously (43).

Mice—C57BL/6J mice were purchased from the Monash Animal Research Platform. NODSCIDIL2R$\gamma^{-/-}$ (NSG) mice were bred in-house. Humanized NODSCIDIL2R$\gamma^{-/-}$ (hung) mice were generated by transplanting 200,000 human CB CD34$^+$ cells with 2×10^6 irradiated CB mononuclear cells into irradiated (2.75 gray, single dose 4 h prior to transplant) NSG mice. Human engraftment was assessed in the peripheral blood 4 weeks post-transplant using anti-human CD45 and anti-mouse CD45. For i-body binding experiments, BM was harvested from huNSG mice by flushing one femur, tibia, and iliac bone as described previously (44). All animals received food and water *ad libitum*. All animal experiments were approved by the Monash Animal Research Platform ethics committee.

Flow Cytometry—Flow cytometric analysis was performed on an LSRII (BD Biosciences), and cell sorting was performed on a Cytopeia Influx (BD Biosciences) as described previously (43). For analysis of human and murine BM and PB, up to 5×10^6 cells were analyzed at 10,000–20,000 cells/s. Data were analyzed using FlowJo 10 software (FlowJo, LLC).

i-Body Binding to Human HSC from CB, BM, and huNSG BM—Human CB and BM CD34$^+$ cells and huNSG BM were stained sequentially with CXCR4 i-bodies (10 μg/ml), anti-His-PE, and an antibody mixture containing CD34-FITC (BD Biosciences catalog no. 348053) and CD38-BV421 (BD Biosciences Horizon catalog no. 562444), washed with PBS (0.5% BSA), and analyzed by flow cytometry as described above. For analysis of huNSG BM, huCD45-PECy7 (BD Biosciences catalog no. 557748) and muCD45-BUV395 (BD Biosciences catalog no. 564279) were also included in the antibody mixture. HSCs from

human CB and BM were defined as CD34$^+$CD38$^-$, and HSCs from huNSG mice were defined as muCD45$^-$huCD45$^+$CD34$^+$CD38$^-$. CB and BM samples from three individual donors and BM from three individual huNSG mice were assessed.

Mobilization of CD34$^+$ Stem and Progenitor Cells in huNSG Mice—HuNSG mice were injected subcutaneously with PBS ($n = 3$), i-body control (10 mg/kg, $n = 3$), AM3-114 (10 mg/kg; $n = 4$), AM3-523 (10 mg/kg; $n = 3$), or AMD3100 (3 mg/kg; $n = 3$). After 1 h, PB was harvested, and WBC were enumerated, red cells lysed, and WBC labeled with anti-human CD45-PB (Biolegend catalog no. 304029), anti-mouse CD45-BV650 (BD Horizon catalog no. 563410), and anti-human CD34-PECy7 (BD Biosciences catalog no. 348791). Human stem and progenitors were defined as muCD45$^-$huCD45$^+$huCD34$^+$, and validation of HSC mobilization by CXCR4 i-bodies was based on a significant increase in CD34$^+$ cells in PB compared with the control i-body and compared with AMD3100-mobilized controls as described previously (45).

i-Body Binding to Murine Hematopoietic Stem and Progenitors—BM cells from C57BL/6J mice were harvested, lineage-depleted, and FACS sorted for LSK progenitor cells, as described previously (43) Sorted LSK cells (from three individual mice) were stained sequentially with CXCR4 i-bodies (10 μg/ml) and anti-His-PE, washed, and analyzed by flow cytometry.

Mobilization of Murine Hematopoietic Stem and Progenitors—C57BL/6J mice were injected subcutaneously with PBS, CXCR4 i-bodies (10 mg/kg), or AMD3100 (3 mg/kg) (5 mice/group for each group). After 1 h mice, were euthanized; the PB was harvested and enumerated; red blood cells were lysed, and WBC were labeled for lineage markers using anti-CD3-PB (Biolegend catalog no. 100214), anti-B220-PB (Biolegend catalog no. 103227), anti-B220-AF647 (Biolegend catalog no. 103226), anti-Gr1-AF647 (Biolegend catalog no. 108418), and anti-Mac1-AF647 (Biolegend catalog no. 101218), as well as stem cell markers using anti-Sca-1-PECy7 (Biolegend catalog no. 122514) and anti-c-kit-BUV395 (BD Biosciences catalog no. 564011) and analyzed as described above. Hematopoietic stem and progenitor cells were defined as L̲in$^-$, S̲ca-1$^+$, c-k̲it$^+$ (LSK).

Sample Size, Statistical Analysis and Blinding

All statistics were performed using GraphPad Prism software (GraphPad Software Inc.). For all experiments, excluding ELISAs and panning, the investigators were blinded to i-body identity (including control i-body) but not to the identity of AMD3100 or vehicle controls. Investigators conducting SPR residual activity in the thermal and pH stability assay analyses were blinded to treatment conditions. At least three independent investigators assessed data arising from all experiments. BM, CB, and HSC data were analyzed using one-way analysis of variance, and where there were statistically significant differences between group means, a follow-up multiple comparisons analysis using the Holm-Sidak approach was performed. $p < 0.05$ was considered significant.

Results

Engineering the i-Body Scaffold—The first crystallographic structures of V_{NAR} revealed close structural similarity with the immunoglobulin domains of the rat neural cell adhesion molecule (NCAM; PBD code 1QZ1) (12). As an initial step in protein engineering the I-set NCAM domain 1 as a humanized binding reagent, we expressed human NCAM immunoglobulin domain 1 as a recombinant protein (termed i-body scaffold). Crystallization of this domain (designated i-body 21H-5, PDB code 5AEA) revealed high homology to the rat NCAM1 Ig domain, with a root mean square deviation of 1.2 Å over 99 α-carbon atoms (Fig. 1, *A* and *B,* and supplemental Table S1). Characteristic of members of the immunoglobulin superfamily, each structure included two sheets of anti-parallel β-strands and a canonical disulfide bond located between residues Cys-22 and Cys-77.

These data suggested that it would be possible to engineer this Ig domain protein by inserting two loops of random amino acids in the corresponding positions that the CDR1 and CDR3 would occupy in the V_{NAR}. To investigate whether the thermal stability of the i-body scaffold was similar to that of a V_{NAR}, we conducted circular dichroism (CD) spectroscopy at 20 and 80 °C. As expected, the spectrum was typical of a predominantly β-strand protein (supplemental Fig. S1*A*, *blue trace*), and heating to 80 °C disrupted this structure to a random coil conformation, as indicated by a significant decrease in ellipticity at 205 nm (supplemental Fig. S1*A*, *red trace*). Consistent with other high stability V-domains (7, 8), the i-body reassumed a β-strand conformation upon cooling (supplemental Fig. S1*A*, *black trace*), a process that could be repeated without apparent loss of protein due to precipitation (*gray traces*), suggesting that the protein scaffold is very stable at high temperatures due to an ability to refold, most likely aided by the internal disulfide bond. V_{NAR} antigen binding capability resides predominantly in the loop regions analogous to antibody CDRs 1 and 3 (46). To assess the feasibility of wild-type human NCAM domain 1 to accommodate similar variability in these regions, i-body 21H-5 was modeled to determine the best framework junction residues for mutation, and the resulting clone 23B-2 was constructed by grafting the CDR3 loop from a previously reported V_{NAR} (clone 1A-7 (34)) onto the 21H-5 "scaffold." The resulting chimeric recombinant protein was soluble, stable, and bound the target antigen (monoclonal antibody 5G8) specifically as measured by ELISA (supplemental Fig. S2).

As proof-of-principle of i-bodies as single domain binding reagents, a small library was then constructed by inserting random sequences of 15 residues in the region corresponding to CDR3. This "15-mer" i-body library was phage-displayed, selected on the monoclonal antibody 5G8, and analyzed for the diagnostic 5G8 recognition sequence (A/S)YP (28, 34). Such i-bodies containing this target sequence were successfully enriched (supplemental Table S2), and one such i-body (designated AD5G8-5; 180 nM affinity for antigen) was produced as a recombinant protein and utilized for a more extended series of characterization experiments that demonstrated the i-body was an extremely stable monomeric protein (supplemental Fig. S1). Specifically, AD5G8-5 solubility was unaffected by short
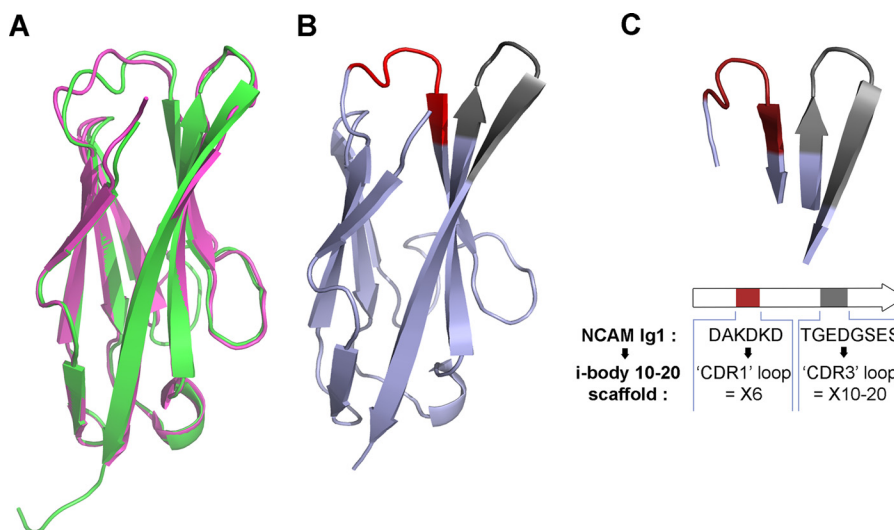
FIGURE 1. **Attributes of the i-body scaffold.** *A,* overlay of the crystal structure of 21H-5 (human NCAM1, Ig1 domain (clone 21H-5, *green*)) and rat NCAM1 Ig1 (PDB 1QZ1, *pink*). *B,* ribbon diagram of the crystal structure of 21H-5 (human NCAM1, Ig1 domain) showing in *red* and *gray* the loops designated as CDR1 and CDR3, respectively. *C, red* and *gray* loops extending from the top of the molecule were replaced, respectively, with fully randomized 6-residue "CDR1" and 10–20-residue "CDR3" antigen-binding loops to produce the i-body scaffold.
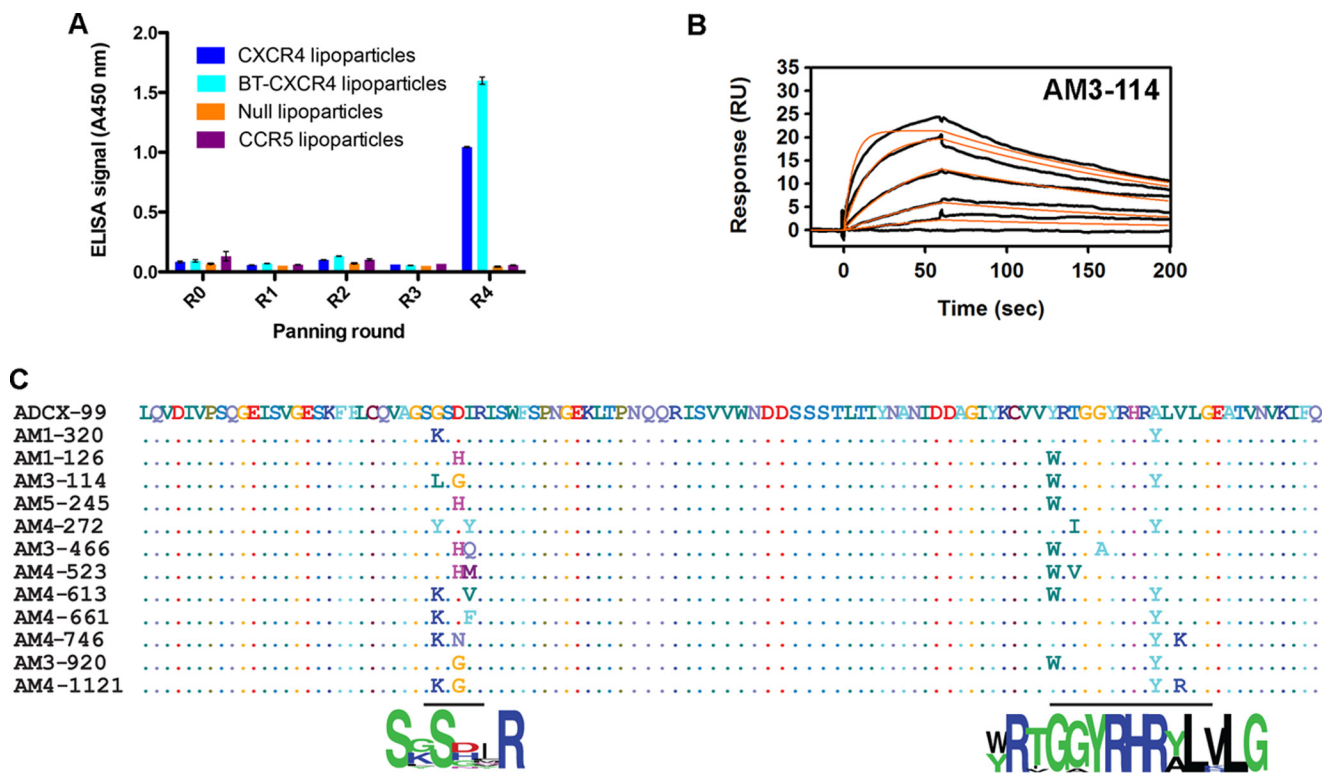

FIGURE 2. **Isolation of CXCR4 binders.** *A,* ELISA of phage particles from sequential panning rounds, showing enrichment of i-bodies with specificity for CXCR4 lipoparticles. *B,* kinetic data set collected for AM3-114 binding to immobilized CXCR4. Injected concentrations were 81, 27, 9, 3, and 1 nM. Binding responses (*black sensorgrams*) are overlaid with fits of a simple 1:1 kinetic interaction model (*orange lines*). *C,* sequence alignment of CXCR4 i-bodies. ADCX-99 was isolated from the primary i-body library. Clones from the first affinity-matured library were AM1-126 and AM1-320. Clones from the second affinity-matured library were AM3-114, AM5-245, AM4-272, AM3-466, AM3-523, AM4-613, AM4-661, AM4-746, AM3-920, and AM4-1121. The sequence LOGO motifs show sequence conservation of residues within the CDRs.

term heat treatment (supplemental Fig. S1*B*), and a thermal and pH stability study demonstrated that retention of active protein was ≥70% at a range of pH values. At 37 °C, retention of active protein was >90% at pH 4 and 5.5, >65% at pH 7.4, and then decreased to >55% at pH 10 (supplemental Fig. S1*C*). Continuous size distribution analysis of analytical ultracentrifugation data yielded excellent fits under all conditions tested. The data

showed that 21H-5 and AD5G8-5 exist as monomers in solution with apparent molar masses of 13.4 and 14.5 kDa, respectively (supplemental Fig. S1*D*). These values are in agreement with the theoretical molecular mass derived from amino acid sequences.

A second generation i-body library was then constructed. Given that the modified NCAM scaffold was shown to have

superior stability, we replaced the 21H-5 residues DAKDKD with a random 6-mer sequence and the 21H-5 residues TGEDGSES with a random sequence that varied between 10 and 20 residues in length (Fig. 1*C*). The positioning of these loops corresponded to the CDR1 and CDR3 regions of the V_{NAR}, respectively, meaning that the resulting molecules could be viewed as essentially humanized equivalents of the single Ig domain of the shark. Based on these specifications, a synthetic combinatorial i-body library was generated.

Identification and Engineering of Selective CXCR4 Binding i-Bodies—Following four rounds of biopanning against lipoparticles harboring the full-length human CXCR4 GPCR protein, enrichment of i-bodies specific for lipoparticles presenting CXCR4 but not CCR5 (another GPCR) was observed (Fig. 2*A*). Analysis of 24 single clones showed strong selective binding to CXCR4 lipoparticles for the vast majority of the clones. DNA sequence analysis revealed this response was predominantly from multiple replicates of a clone that was subsequently designated as "ADCX-99." Several other panning campaigns were performed, incorporating subtle variations in washing regimes, antigen presentation, and the use of CXCR4-expressing cells, resulting in a diverse range of i-body sequences being identified. However, ADCX-99 was pursued for further studies as it showed superior protein expression levels.

Surface plasmon resonance revealed that ADCX-99 had relatively weak affinity (~650 nM) for CXCR4 lipoparticles (Table 1 and supplemental Fig. S3*A*). To improve the affinity of ADCX-99 enough to generate i-bodies with relevant therapeutic potential, the ADCX-99 sequence was subjected to two iterative rounds of affinity maturation in which mutations were introduced in the CDR1 and CDR3. In the first round of affinity maturation (AM1), the mutation rate was set at 0 or 1 amino acid mutation per CDR loop, or the C-terminal region of ADCX-99 (including CDR3) was recombined by splice overlap PCR with the N-terminal region (including CDR1) of the entire i-body library. Following biopanning of these AM1 libraries and screening of ~2,000 clones, SPR analysis showed significant improvement in binding kinetics of a panel of 90 clones. Of these, the most notable were clones AM1−126 and AM1−320, which had affinities of 27 and 16 nM, respectively (Table 1 and supplemental Fig. S3, *B and C*), representing a 24−40-fold improvement in affinity. On comparing the panel of AM1 affinity matured clones, it was evident that four residue positions were critical for conferring the improved affinity for CXCR4, namely residues 28 and 30 in CDR1 and residues 80 and 89 in CDR3 (Fig. 2*C*). Accordingly, in the second round of affinity maturation, the AM2 affinity matured libraries were constrained such that position 28 consisted of Tyr or Lys residues only, position 30 by His or Gly, and positions 80 and 89 consisted of only Trp or Tyr, respectively, and other positions in the CDRs were subjected to random mutation, with a maximum of 2 residues mutated per clone. Following biopanning of the AM2 libraries, SPR analysis of selected i-bodies showed further improvement in affinity in the low nanomolar range (Table 1, Fig. 2*B*, and supplemental Fig. S3, *D−G*). Interestingly, all the selected i-bodies retained the positively charged arginine residue in their CDRs (Fig. 2*C*), consistent with the view that the CDR3 could penetrate into the negatively charged binding

TABLE 1
Attributes of the panel of CXCR4 i-bodies
ADCX-99 was isolated from the primary i-body library. AM1-126 and AM1-320 were isolated from the first affinity maturation library. AM3-114, AM4-272, AM3-523, AM4-746, and AM4-1121 were from the second affinity matured library.

| i-Body	Mutations		Binding kinetics determined by SPR			IC$_{50}$ in β-arrestin BRET assay[a] (μM) ± S.D.	IC$_{50}$ in calcium^{2+} flux assay[b] (μM) ± S.D.	IC$_{50}$ in cAMP assay[c] (mean, nM)	HIV entry inhibition IC$_{50}$ (nM ± S.D.)
	CDR1	CDR3	Affinity K_D (nM) ± S.D.	Association rate constant $k_a \times 10^5$ (M^{-1}s^{-1}) ± S.D.	Dissociation rate constant $k_d \times 10^{-3}$ (s^{-1}) ± S.D.				
ADCX-99	None	None	643 ± 35	—[d]	—[d]	No activity	—	—	—
AM1-126	D30H	Y80W	27.2 ± 4.8	5.5 ± 1.5	14.6 ± 1.4	—	—	—	—
AM1-320	G28K	A89Y	15.9 ± 0.1	7.9 ± 0.6	12.6 ± 0.9	—	—	—	—
AM3-114	G28L, D30G	Y80W, A89Y	4.2 ± 1.2	15.9 ± 6.4	4.4 ± 0.1	1.18 ± 1.27	μM range[a]	99	131 ± 25
AM4-272	G28Y, I31Y	T82I, A89Y	1.8 ± 0.2	82.2 ± 2.2	14.5 ± 2.0	1.38 ± 0.87	BLD	300	838 ± 77
AM3-523	D30H, I31M	Y80W, T82V	9.2 ± 0.3	9.8 ± 0.2	9.1 ± 0.1	2.94 ± 2.07	μM range[a]	225	349 ± 16
AM4-746	G28K, D30N	A89Y, V91K	4.0 ± 1.9	34.7 ± 13.6	12.6 ± 1.1	2.04 ± 1.54	BLD[e]	115	148 ± 19
AM4-1121	G28K, D30G	A89Y, V91R	6.3 ± 0.6	17.0 ± 4.0	10.7 ± 1.6	1.04 ± 0.38	μM range[a]	125	115 ± 9
AMD3100	—	—	18.5[f]	5.46[f]	10.1[f]	0.037 ± 0.033	0.31	6.15	10.3[c]
Control i-body	—	—	—	—	—	—	μM range	No activity	>1000[c]

[a] Very weak activity is shown; IC$_{50}$ could not be determined.
[b] Mean of duplicates is shown.
[c] S.D. was not determined as assay was not replicated.
[d] Rate parameters were not available as steady state model was used to derive affinity.
[e] BLD means below the limit of detection.
[f] Data are from Heym *et al.* (75).
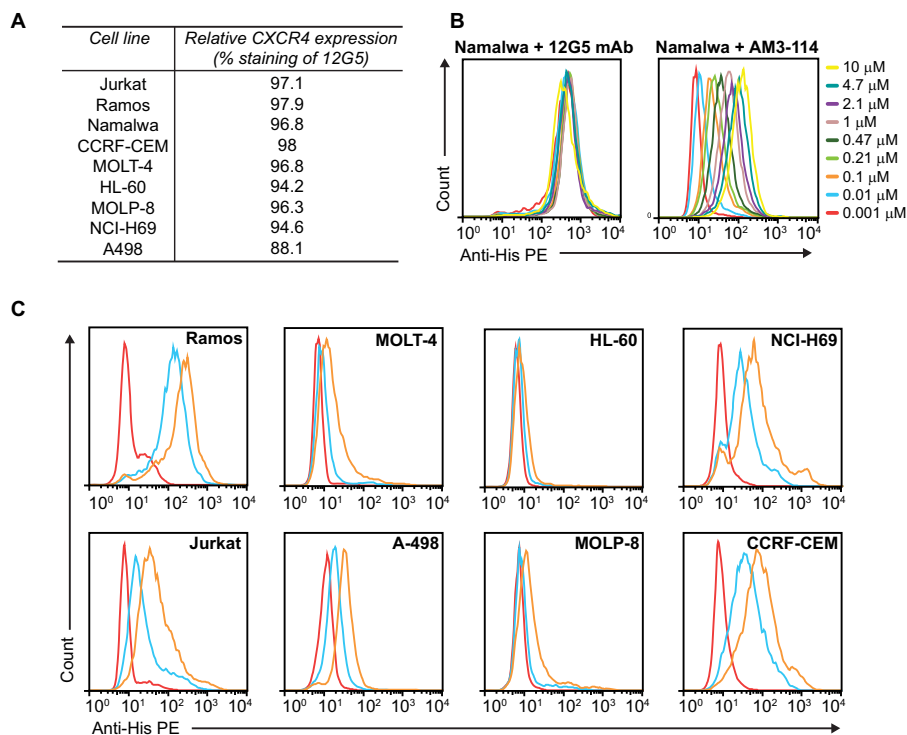
FIGURE 3. **Titration of AM3-114 binding to CXCR4-positive cancer cell lines.** *A,* percent of various cell lines stained with 12G5, indicating relative expression level of CXCR4 for each cell line. *B,* Namalwa cells were treated with anti-CXCR4 mAb 12G5 or AM3-114 at various concentrations, and then staining was analyzed by flow cytometry. *C,* various cell lines were treated with AM3-114 at 10 μM, *orange trace*; 1 μM, *blue trace*; 0.001 μM, *red trace*, and then staining was visualized by flow cytometry.

pocket of CXCR4 (47). An SPR-based method to assess whether the affinity-matured i-bodies were able to compete with CXCL12 for binding to CXCR4 indicated that certain higher affinity i-bodies (notably AM3-114) were able to reduce the CXCL12-binding response (supplemental Fig. S3, *H–L*) but not block it completely. We deduced that because CXCL12 initially binds rapidly to the flexible N-terminal loop of CXCR4 and then subsequently to the transmembrane region (48), it is conceivable that a CXCR4 molecule could bind both an i-body and CXCL12 at the same time, and hence only modest competition was observed in this assay.

i-Bodies Bind Cancer Cell Lines and Inhibit Cell-mediated Signaling—A panel of five of the highest affinity i-bodies, all with single digit nanomolar affinity for CXCR4 (AM3-114, AM4-272, AM3-523, AM4-746, and AM4-1121, see Table 1) was further characterized in a variety of *in vitro* assays. As a first step in determining whether AM3-114 could also recognize CXCR4-expressing cells, flow cytometry was used to visualize the binding of the this i-body to a panel of CXCR4-positive cancer cell lines (Fig. 3). AM3-114 showed dose-dependent but variable binding to all cell lines, except HL-60 where little binding was observed. The variable binding is perhaps a function of the observation that GPCR conformation and tissue/cell type can markedly affect ligand binding and activity (49, 50).

With our *in situ* data showing a strong correlation between cell-surface CXCR4 expression levels and i-body binding, it was important to assess the specificity of the i-bodies for CXCR4 relative to other chemokine receptors. i-body-mediated antagonism of a panel of 19 chemokine receptors expressed on PathHunter cells (DiscoveRx) was monitored by β-arrestin activa-

tion (Fig. 4). Activation of chemokine receptors other than CXCR4 was low, *i.e.* the background signal for most other receptor/i-body combinations was <20% for all i-bodies. As anticipated, most i-bodies principally recognized CXCR4 rather than the other chemokine receptors. Specifically, AM1-126, AM1-320, AM3-523, AM4-746, and AM4-1121 elicited strong (>50%) β-arrestin inhibition, with AM3-523 showing the strongest inhibition (>90%). AM3-114 and AM4-272 elicited comparatively weak activation of β-arrestin inhibition in the CXCR4 model at 10 and 24%, respectively. Despite the limitations of this high throughput screen format (*i.e.* single i-body concentration tested, conducted in singlicate), it was clear that the i-bodies were highly specific for CXCR4 and were thus evaluated in further detail.

Given the specificity of the panel of i-bodies for CXCR4, and in an effort to extend our analysis of antagonism of β-arrestin recruitment, a series of i-body dose-response assays were conducted using BRET technology (40) in cells transiently expressing human CXCR4/Rluc8 and β-arrestin2/Venus in the presence of 100 nM CXCL12 agonist (Fig. 5A and Table 1). AMD3100 was a potent antagonist in the assay. Although the parent CXCR4 i-body, ADCX-99, had a very weak effect on β-arrestin recruitment, the affinity-matured i-body panel was clearly antagonistic in the low micromolar range (Table 1), thus reflecting SPR binding kinetics results and further validating the affinity maturation strategy.

The panel of CXCR4 i-bodies was examined in *in vitro* assays for the ability to intervene with stimulation of CXCR4 by CXCL12, as measured by changes in intracellular calcium and cAMP levels. The previously described antagonist AMD3100
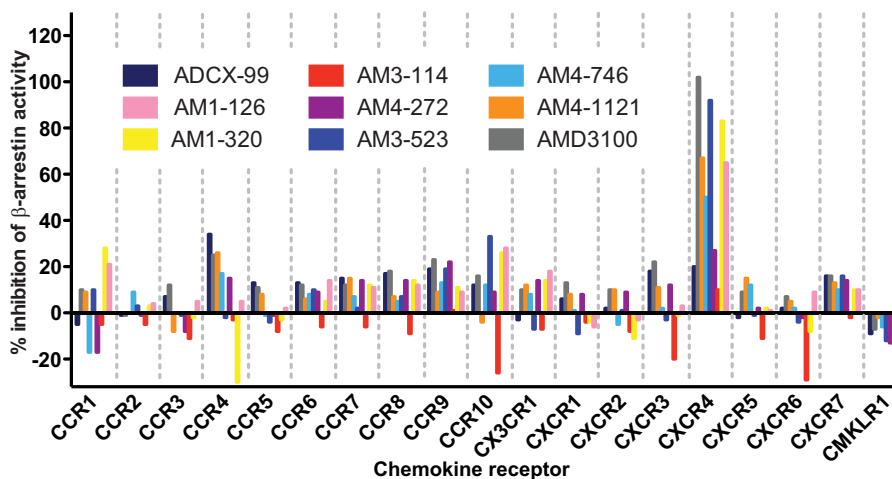
FIGURE 4. **Chemokine receptor screen with CXCR4 i-bodies.** β-Arrestin activation following chemokine receptor stimulation in the presence of ADCX-99, AM1-126, AM1-320, AM3-114, AM4-272, AM3-523, AM4-746, AM4-1121, and AMD3100. The assay was conducted once with i-bodies, and AMD3100 was tested at a single concentration.
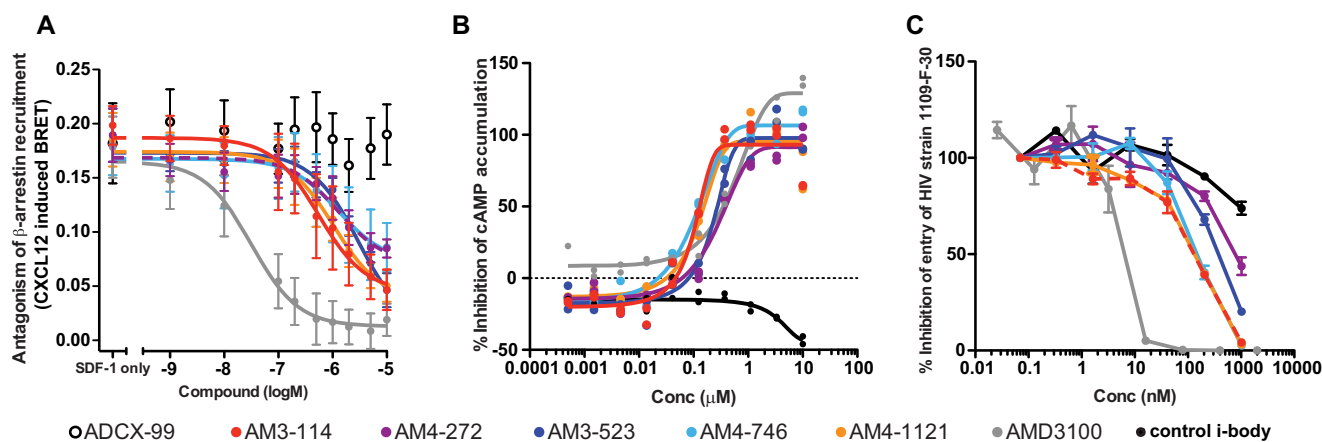

FIGURE 5. **Characterization of CXCR4 i-bodies in β-arrestin, cAMP, and HIV assays.** *A,* inhibition of β-arrestin recruitment to CXCR4 in HEK293FT cells transiently transfected with CXCR4/Rluc8 and β-arrestin2/Venus as measured by BRET. Cells were stimulated for $\sim$20 min with 100 nM CXCL12 in the presence of increasing concentrations of ADCX-99, AM3-114, AM4-272, AM3-523, AM4-746, AM4-1121, and AMD3100. *Error bars* show S.E. *B,* % inhibition of cAMP production in CHO-K1 cells expressing CXCR4 following stimulation with CXCL12 at EC$_{80}$ (3.2 nM), in the presence of AM3-114, AM4-272, AM3-523, AM4-746, AM4-1121, and AMD3100. The line of best fit connects the duplicate data points for each test condition. *C,* % inhibition of entry of HIV luciferase reporter viruses pseudotyped with 1109-F-30 Env in the presence of AM3-114, AM4-272, AM3-523, AM4-746, AM4-1121, and AMD3100 and a control i-body. *Error bars* show S.D.

displayed a dose-dependent effect in both assays. In a recombinant human CXCR4 Gαqi5 chimeric cell line none of the CXCR4 i-bodies blocked calcium flux, whereas AMD3100 inhibited flux quite potently (Table 1) consistent with a previous report (51). By comparison, the i-bodies were effective at blocking the CXCL12-induced decrease in cAMP in CHO-1 cells. Indeed, all i-bodies were equivalent to or slightly more potent than AMD3100 in this assay (Fig. 5*B* and Table 1).

CXCR4 i-Bodies Inhibit HIV Entry—Because it has been reported that some strains of HIV use CXCR4 as a co-receptor for viral entry and that CXCR4 antagonists, such as AMD3100, are capable of blocking entry of the virus (52), it was of interest to establish whether the i-bodies could modulate HIV infectivity. We investigated the potency of the CXCR4 i-body panel in an inhibition assay using luciferase reporter viruses pseudotyped with a CXCR4-using envelope of HIV, the primary strain 1109-F-30, which is a subtype C clinical envelope from a chronically infected individual (53). All of the CXCR4 i-bodies

showed significant levels of inhibition of this strain (Fig. 5*C*). i-bodies AM3-114, AM4-746, and AM4-1121 were most effective at inhibiting entry (Table 1 and Fig. 5*C*). By comparison, AMD3100 was more potent than the i-bodies, and the control i-body, which does not bind CXCR4, had little effect on strain 1109-F-30. The i-bodies did not inhibit entry of reporter viruses pseudotyped with VSVG, which is the envelope from the vesicular stomatitis virus that undergoes endocytosis after binding to an unrelated receptor (supplemental Fig. S4*A*), and were also not able to block HIV entry into host cells by a strain of HIV (YU-2) that relies on CCR5 for entry (supplemental Fig. S4*B*), therefore demonstrating that the anti-CXCR4 activity of the i-bodies is critical for blocking HIV entry.

Despite the variations in conditions among these *in vitro* assays (cell type, agonist concentration, etc.), the CXCR4 i-body panel appeared to show specific activity in cAMP, β-arrestin recruitment, and HIV assays but not in the calcium flux assay. Overall, AM3-114 generally showed the strongest potency. Variation among the individual i-body binders was observed in each assay,

TABLE 2
Important residues for i-body binding to CXCR4

Important residues (where lower numbers represent weaker binding to specific CXCR4 mutants) were identified and categorized into three groups based on reactivity values, (54, 55). Primary critical residues (black shading) make the highest energetic contributions to the interaction; secondary critical residues (dark gray shading) contact residues with lower energy or may affect the presentation of the epitope; and tertiary critical residues (light gray shading) appear to affect the binding of the i-body but with no clear distinction as to how or why.

CXCR4 mutation	AM3-114	AM4-272	AM3-523
E32K	58.8	38.1	6.6
V112A	63.6	109.4	7.6
Y184S	96.1	61.7	12.6
F189L	26.1	21.8	45.5
D193G	37.8	80.1	78.6
W195R	28.8	84.8	57.6
D262G	30.2	26.7	12.5
L266H	23.6	60.6	60.4
E288G	54.6	80.6	91.5

which was intriguing, and further studies are required to confirm the extent and significance of this.

AM3-114, AM3-523, and AM4-272 Recognize Overlapping but Distinct Residues in the CXCR4 Binding Pocket—To gain a better understanding of the precise nature of the interaction between the i-bodies and CXCR4, we decided to elucidate the epitopes for i-bodies AM3-114, AM4-272, and AM3-523 using Integral Molecular's CXCR4 Shotgun Mutagenesis technology platform. To produce the CXCR4 library, each residue of the GPCR was individually mutated to produce a mutant library of 733 different clones. The mutants were then ranked for ability to bind each of the three CXCR4 i-bodies. A number of primary or critical CXCR4 residues whose side chains make the highest energetic contributions to the interaction between each i-body and the GPCR (54, 55) were identified for each i-body, and additional secondary and tertiary residues that impart important but lower energetic contributions were also identified (Table 2). It was evident that the three i-bodies all bound in the CXCL12 binding pocket of CXCR4, which is located in the extracellular domain of the receptor (Fig. 6). Interestingly, the primary or critical binding residues were somewhat overlapping, although distinct for the three i-bodies. The critical residues for AM3-114 and AM3-523 are the most distinct, whereas those of AM4-272 are intermediate between the two (Fig. 6). Mutation of Asp-262 (located in the major binding pocket) to glycine negatively impacts the binding of all three i-bodies, suggesting they all appear to bind in the CXCR4 binding pocket. Interestingly, Asp-262 is a key residue that is contacted by the small molecule AMD3100 (56), consistent with the drug-like properties of the i-bodies. Few of the mutated residues that reduce the binding of i-bodies affected the binding of nanobodies 238D2 and 238D4 (6), suggesting that the i-body and the nanobody contact sites on CXCR4 are different. In fact, of the 11 critical residues contacted by the nanobodies, 10 of them are in ECL2 and 1 in ECL3, some distance from the ligand binding

pocket. Mutation of the residues on CXCR4 critical for binding the human CXCR4 mAb 12G5 (Glu-179, Asp-181, Asp-182, Tyr-190, and Cys-274) (57) did not affect i-body binding.

i-Bodies Block Cell Recruitment in a Mouse in Vivo Model—i-Body efficacy in a murine *in vivo* study was performed by examining whether the i-bodies could antagonize cell recruitment in an "air pouch" model (58). In this study, the vehicle-only control showed extensive leukocyte migration into the air pouch in response to the presence of CXCL12 (Fig. 7A), whereas all anti-CXCR4 i-bodies were found to substantially block this migration, with AM3-114 being the most effective. As expected, AMD3100 was also able to inhibit CXCL12-induced infiltration of leukocytes into the air pouch, and a non-CXCR4-binding i-body had no effect. These data indicate the i-bodies are able to engage CXCR4-expressing immune cells in the peripheral blood and block their infiltration toward an inflammatory signal.

CXCR4 i-Bodies Bind to but Do Not Mobilize Hematopoietic Stem Cells—AMD3100 has previously been shown to rapidly mobilize long term repopulating HSCs in both primates and mice (59, 60). To determine whether CXCR4 i-bodies bind HSC, *in vitro* binding analysis to human $CD34^+CD38^-$ cells was assessed (Fig. 7B). i-Bodies AM3-114, AM4-272, and AM3-523 effectively bound human CB HSC with similar affinity (Fig. 7C). AM3-114 also effectively bound to human BM HSC and BM harvested from humanized NODSCIDIL2Rγ$^{-/-}$ (huNSG) mice (Fig. 7D). To determine whether i-bodies mobilized human hematopoietic stem and progenitors, huNSG mice were treated with CXCR4 i-bodies, and PB was analyzed for human $CD34^+$ cells. In contrast to AMD3100, which effectively mobilized $CD34^+$ cells, neither AM3-114 nor AM3-523 showed any evidence of stem cell mobilization (Fig. 7E).

To assess whether i-bodies AM3-114, AM4-272, and AM3-523 also bound murine hematopoietic stem and progenitor cells, isolated LSK BM cells were labeled with CXCR4 i-bodies (Fig. 8, A–C). Although AM3-523 did not bind murine LSK cells, low but significant levels of binding were detected using AM3-114 and AM4-272 (Fig. 8, B and C). To determine whether CXCR4 i-bodies were capable of mobilizing murine hematopoietic stem cells and progenitors, LSK cells in the PB of C57BL/6 mice were assessed as evidence for stem cell mobilization (Fig. 8, D–F). Following the administration of AM3-114, AM4-272, AM3-523, AM4-746, or AM4-1121, no significant increase in WBC cellularity (Fig. 8E) or LSK cell numbers was detected in the PB (Fig. 8F). As expected, the administration of AMD3100 resulted in significant increases in PB WBC (Fig. 8F) and LSK cells (Fig. 8F). The lack of stem cell mobilization following CXCR4 i-bodies is consistent with results obtained using huNSG mice. Thus, our results show that although CXCR4 i-bodies are capable of binding BM HSC, they are unable to induce their mobilization, further confirming that CXCR4 i-bodies are mechanistically and physiologically distinct from the canonical CXCR4 antagonist AMD3100.

Discussion

GPCRs are complex membrane proteins that control multiple signaling pathways, and it is well established that obtaining monoclonal antibodies against GPCRs is not trivial (61–63). At
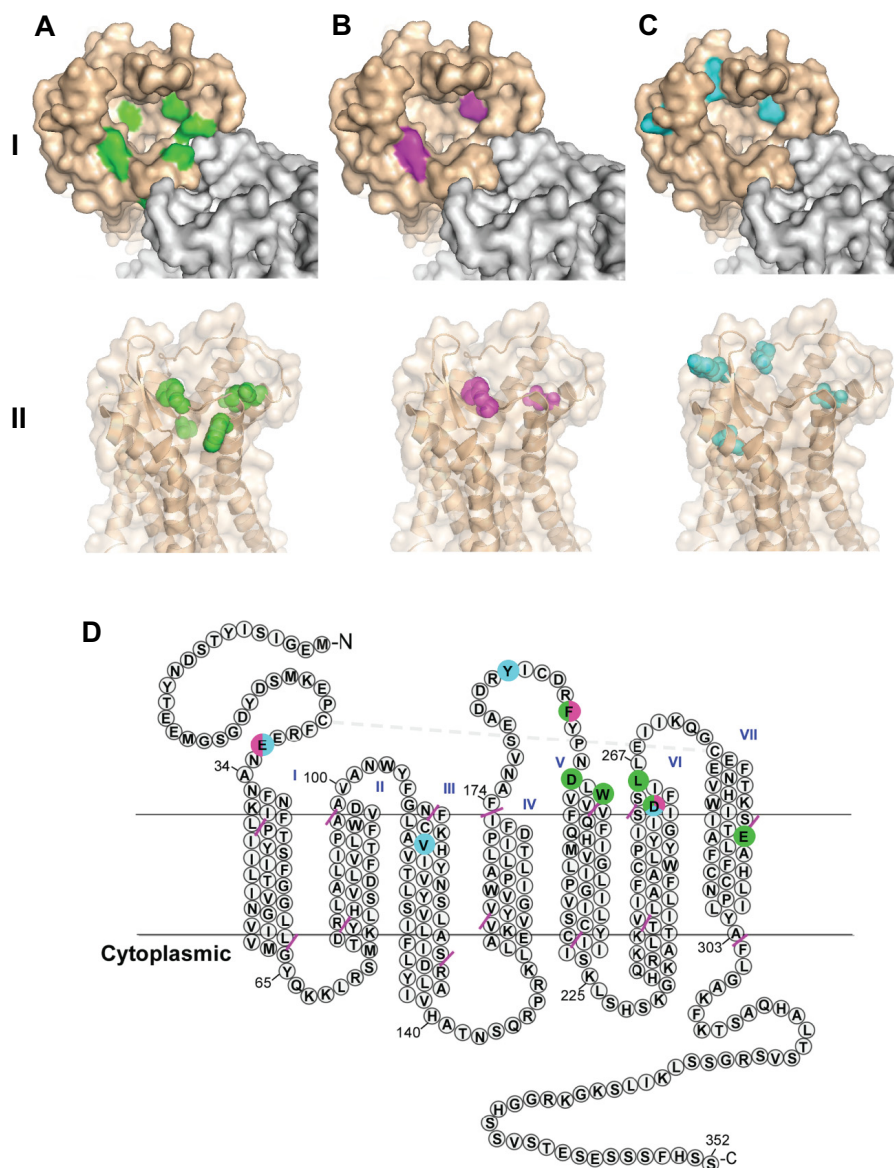
FIGURE 6. **Epitope mapping i-body binding to CXCR4.** Epitope mapping of i-bodies AM3-114, AM4-272, and AM3-523 binding to CXCR4 is shown. The primary, secondary, and tertiary contact residues identified for binding of AM3-114 (*A*), AM4-272 (*B*), and AM3-523 (*C*) are highlighted on space-filled depictions of the top view (*panel I*) and side view (*panel II*) of the active site of CXCR4 (derived from PDB 3ODU). *D, snake plot* representation of CXCR4 (derived from PDB 3ODU) showing residues involved in binding to AM3-114 (*green*), AM4-272 (*magenta*), and AM3-523 (*cyan*). The epitope of AM3-114 consists of residues in ECLs 1–3, as well as transmembrane (TM) regions 4 and 7. The epitope of AM4-272 consists of residues in the N terminus, ECL2, ECL3, and TM4. The epitope of AM3-523 consists of residues in N terminus, ECL2, ECL3, and TM3. *Pink dashes* represent membrane boundaries.

a functional level, stimulation of CXCR4 by its ligand CXCL12 is important in homeostasis and embryonic development, as well as homing of stem and progenitor cells in the bone marrow and into the peripheral blood, yet it is also implicated in multiple disease states. These diverse functions make drug development difficult, and prolonged antagonism of the receptor can raise side-effect concerns, including hematopoietic dysfunctions, mobilization of normal progenitor cells, and their exposure to cytotoxic drugs in cancer settings (64). Indeed, the development of AMD3100 for anti-retroviral HIV-1 therapy was discontinued due to side effects, including thrombocytopenia and paresthesia (65).

We describe herein the first report of a human single domain scaffold that has been engineered from the I-set immunoglobulin superfamily, known as the i-body. The scaffold displays

stability profiles that are consistent with other Ig domains, namely thermal and extreme pH stability. Engineering of the scaffold to produce a combinatorial library enabled rapid screening against CXCR4 and yielded i-body binders that were readily affinity-matured to vastly improve binding kinetics.

According to SPR analysis, AM3-114, AM4-272, AM3-523, AM4-746, and AM4-1121 i-bodies were shown to bind human CXCR4 on lipoparticles in the low nanomolar range, and i-bodies AM3-114 and AM3-523 competed somewhat with binding of CXCL12, whereas AM4-272 did not. The i-bodies displayed some disparity of activity in β-arrestin, cAMP, and HIV invasion inhibition assays, although the overall trend was antagonistic. Epitope mapping revealed that AM3-114, AM4-272, and AM3-523 appear to bind in the major subpocket (66) of the receptor and that AM3-114 appears to bind deeper into the
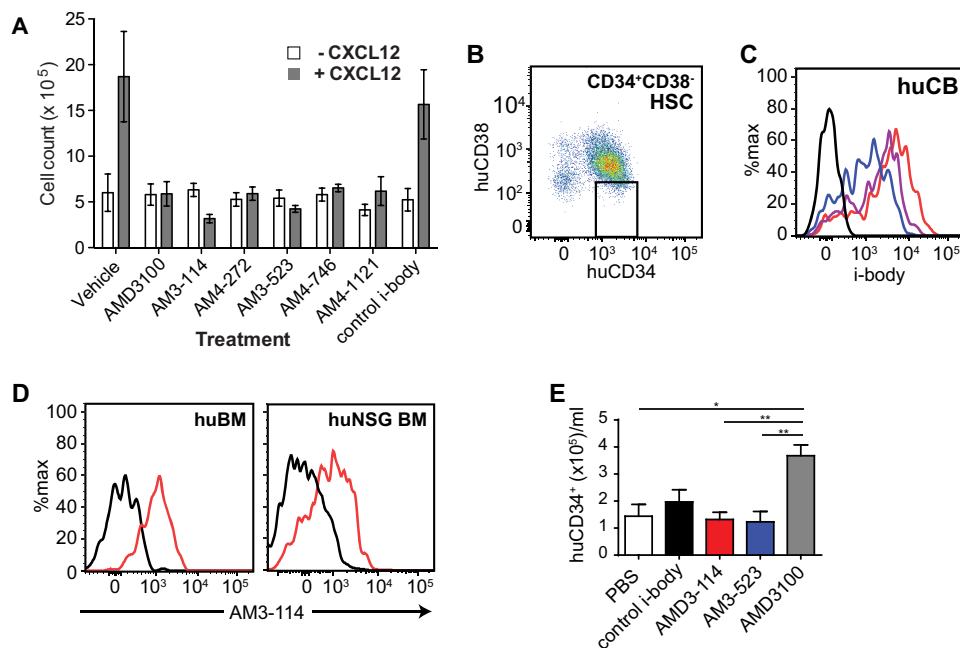
FIGURE 7. **CXCR4 i-bodies bind but do not mobilize human stem and progenitor cells.** *A,* in a murine model, CXCR4 i-bodies blocked cell migration into an artificial skin air-pouch, $n = 5$; *error bars* are expressed as S.E. *B,* representative dot plot of human CD34$^+$CD38$^-$ HSC. *C,* representative flow cytometric histogram of i-body binding to human CB CD34$^+$CD38$^-$ HSC using AM3-114 (*red*), AM4-272 (*purple*), and AM3-523 (*blue*). *D,* representative histogram of AM3-114 (*red*) binding to human BM CD34$^+$CD38$^-$ HSC and muCD45$^-$huCD45$^+$CD34$^+$CD38$^-$ HSC from huNSG BM. Control i-body shown in *black. E,* mobilization of muCD45$^-$huCD45$^+$CD34$^+$ stem and progenitor cells in huNSG mice. *Error bars* are expressed as S.E. *, $p < 0.05$; **, $p < 0.01$, $n = 3$.
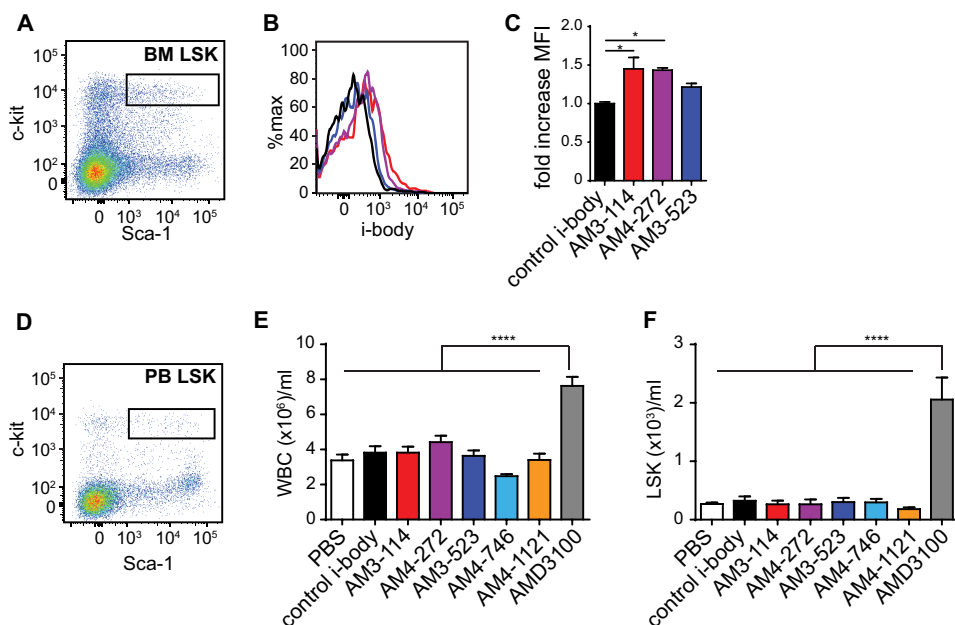
FIGURE 8. **CXCR4 i-bodies do not mobilize murine stem and progenitor cells.** *A,* representative flow cytometry plot of BM LSK progenitors. *B,* representative histogram of i-body binding to sorted murine BM LSK cells using AM3-114 (*red*), AM4-272 (*purple*), and AM3-523 (*blue*). *C,* data in *B* expressed as fold-increase mean fluorescence intensity (*MFI*) relative to control i-body. *D,* representative dot plot of mobilized PB LSK cells. *E,* total WBC. *F,* LSK cell content in PB of mice administered PBS, i-bodies, or AMD3100. *Error bars* expressed as S.E. *, $p < 0.05$; ****, $p < 0.001$, $n = 3$.

active site than any previously reported antibody antagonist. Indeed, comparisons can be drawn between the binding of these i-bodies to CXCR4 and analogues of the gonadotrophin-releasing hormone decapeptide binding to its cognate receptor. Mutagenesis studies of the gonadotrophin-releasing hormone receptor have revealed a particular role for extracellular loop (ECL) 2/TM5/TM6/ECL3 as a region that differentiates binding modes of different ligands (67). Taken

together, these data suggest that i-bodies provide an attractive format for generating a range of highly specific, high affinity binders to a GPCR.

CXCR4/CXCL12 interactions are critical for the homing and retention of stem and progenitor cells in BM, and it is widely accepted that its disruption by CXCR4 inhibitors such as AMD3100 results in the rapid mobilization of long term repopulating HSC (60). A recent study revealed CXCR4-dependent

release of CXCL12 from BM osteoblasts, and endothelial cells is a key mechanism of AMD3100-mediated HSC mobilization (68). Stem and progenitor cell mobilization by AMD3100 was found to involve reactive oxygen species signaling, which results in the release of CXCL12 and subsequent activation of the serine protease urokinase plasminogen activator (68). These data suggest that AMD3100 has additional active roles in the mobilization of stem and progenitor cells that involve CXCR4-dependent downstream signaling. Moreover, although neutralizing CXCR4 and CXCL12 antibodies inhibit steady-state egress of progenitors as well as G-CSF and AMD3100-induced HSC mobilization, they are unable to mobilize stem cells and progenitors themselves (69). Thus, although direct inhibition of the CXCR4/CXCL12 interaction is critical, it only partially accounts for the effects of AMD3100-mediated mobilization. Our data show that although anti-CXCR4 i-bodies bind BM HSC, their modulation of hematopoietic cells is in a manner that is physiologically distinct from AMD3100.

Circulating bone-derived mesenchymal cells have the potential to develop into fibrocytes and can play a critical role in the pathogenesis of fibrosis (70). A murine model of bleomycin-induced pulmonary fibrosis has shown that circulating fibrocytes (characterized by co-expression of CD45 and CXCR4) can traffic to the lungs in response to CXCL12 release (71). Several studies have indicated that CXCR4 inhibitors that do not mobilize stem cells would be useful in long term studies and therapies. Shu *et al.* (72) demonstrated that the CXCR4 antagonist, MSX-122, which does not mobilize stem cells, was much more effective at mitigating fibrosis than AMD3100. Indeed, MSX-122 significantly attenuated the development of fibrosis by 70%, although AMD3100 only trended toward reduction in fibrosis. These researchers noted that there was significant mortality when AMD3100 was administered intraperitoneally or intravenously (up to 50%), although no mortality was seen in MSX-122-treated mice.

It has been postulated that chemokine receptors such as CXCR4 can preferentially activate one of several possible signaling pathways, a concept termed biased signaling or functional selectivity (49, 50). Consequently, there is increasing interest in developing GPCR-specific drugs with novel modalities that are capable of modulating one GPCR signaling pathway over another in a biased manner. Such bias may involve agonism, antagonism, inverse agonism, partial agonism, or allosteric modulation and thus maximizes desired efficacy, reducing unwanted side effects and minimizing toxicity (73). The CXCR4 i-body panel has the potential for development of therapeutic or diagnostic agents following further engineering, for example, to specifically bind the major and/or minor CXCR4 subpocket (as has been demonstrated with the IT1t peptide binding to the minor subpocket (74)) or for specifically targeting one signaling pathway over others.

Author Contributions—K. G., O. D., B. C., S. K. N., P. G., A. P., S. D. N., and M. F. designed the research. K. G., O. D., H. S., M. R., A. P., K. V., K. L., B. L., D. C., T. M. R., M. K., M. D., Y. K., K. P., and J. C. performed the research. K. G., O. D., K. D. G. P., M. R., M. K., C. D., and M. P. analyzed the data. K. G., O. D., B. C., S. K. N., M. R., and M. F. wrote the paper. All authors reviewed the results and approved the final version of the manuscript.

References

1. Shukra, A. M., Sridevi, N. V., Dev, C., and Kapil, M. (2014) Production of recombinant antibodies using bacteriophages. *Eur. J. Microbiol. Immunol.* **4,** 91–98
2. Jost, C., and Plückthun, A. (2014) Engineered proteins with desired specificity: DARPins, other alternative scaffolds and bispecific IgGs. *Curr. Opin. Struct. Biol.* **27,** 102–112
3. Weidle, U. H., Auer, J., Brinkmann, U., Georges, G., and Tiefenthaler, G. (2013) The emerging role of new protein scaffold-based agents for treatment of cancer. *Cancer Genomics Proteomics* **10,** 155–168
4. Wurch, T., Pierré, A., and Depil, S. (2012) Novel protein scaffolds as emerging therapeutic proteins: from discovery to clinical proof-of-concept. *Trends Biotechnol.* **30,** 575–582
5. Rasmussen, S. G., Choi, H. J., Fung, J. J., Pardon, E., Casarosa, P., Chae, P. S., Devree, B. T., Rosenbaum, D. M., Thian, F. S., Kobilka, T. S., Schnapp, A., Konetzki, I., Sunahara, R. K., Gellman, S. H., Pautsch, A., *et al.* (2011) Structure of a nanobody-stabilized active state of the β(2) adrenoceptor. *Nature* **469,** 175–180
6. Jähnichen, S., Blanchetot, C., Maussang, D., Gonzalez-Pajuelo, M., Chow, K. Y., Bosch, L., De Vrieze, S., Serruys, B., Ulrichts, H., Vandevelde, W., Saunders, M., De Haard, H. J., Schols, D., Leurs, R., Vanlandschoot, P., *et al.* (2010) CXCR4 nanobodies (VHH-based single variable domains) potently inhibit chemotaxis and HIV-1 replication and mobilize stem cells. *Proc. Natl. Acad. Sci. U.S.A.* **107,** 20565–20570
7. Griffiths, K., Dolezal, O., Parisi, K., Angerosa, J., Dogovski, C., Barraclough, M., Sanalla, A., Casey, J. L., González, I., Perugini, M. A., Nuttall, S., and Foley, M. (2013) Shark variable new antigen receptor (VNAR) single domain antibody fragments: stability and diagnostic applications. *Antibodies* **2,** 66–81
8. Liu, J. L., Zabetakis, D., Brown, J. C., Anderson, G. P., and Goldman, E. R. (2014) Thermal stability and refolding capability of shark derived single domain antibodies. *Mol. Immunol.* **59,** 194–199
9. Walsh, R., Nuttall, S., Revill, P., Colledge, D., Cabuang, L., Soppe, S., Dolezal, O., Griffiths, K., Bartholomeusz, A., and Locarnini, S. (2011) Targeting the hepatitis B virus precore antigen with a novel IgNAR single variable domain intrabody. *Virology* **411,** 132–141
10. Goodchild, S. A., Dooley, H., Schoepp, R. J., Flajnik, M., and Lonsdale, S. G. (2011) Isolation and characterisation of Ebolavirus-specific recombinant antibody fragments from murine and shark immune libraries. *Mol. Immunol.* **48,** 2027–2037
11. Nuttall, S. D. (2012) Overview and discovery of IgNARs and generation of VNARs. *Methods Mol. Biol.* **911,** 27–36
12. Streltsov, V. A., Varghese, J. N., Carmichael, J. A., Irving, R. A., Hudson, P. J., and Nuttall, S. D. (2004) Structural evidence for evolution of shark Ig new antigen receptor variable domain antibodies from a cell-surface receptor. *Proc. Natl. Acad. Sci. U.S.A.* **101,** 12444–12449
13. Chatterjee, S., Behnam Azad, B., and Nimmagadda, S. (2014) The intricate role of CXCR4 in cancer. *Adv. Cancer Res.* **124,** 31–82
14. Moll, N. M., and Ransohoff, R. M. (2010) CXCL12 and CXCR4 in bone marrow physiology. *Expert Rev. Hematol.* **3,** 315–322
15. Feng, Y., Broder, C. C., Kennedy, P. E., and Berger, E. A. (1996) HIV-1 entry cofactor: functional cDNA cloning of a seven-transmembrane, G protein-coupled receptor. *Science* **272,** 872–877
16. Hummel, S., Van Aken, H., and Zarbock, A. (2014) Inhibitors of CXC chemokine receptor type 4: putative therapeutic approaches in inflammatory diseases. *Curr. Opin. Hematol.* **21,** 29–36
17. Lukacs, N. W., Berlin, A., Schols, D., Skerlj, R. T., and Bridger, G. J. (2002) AMD3100, a CXCR4 antagonist, attenuates allergic lung inflammation and airway hyperreactivity. *Am. J. Pathol.* **160,** 1353–1360

18. Avniel, S., Arik, Z., Maly, A., Sagie, A., Basst, H. B., Yahana, M. D., Weiss, I. D., Pal, B., Wald, O., Ad-El, D., Fujii, N., Arenzana-Seisdedos, F., Jung, S., Galun, E., Gur, E., and Peled, A. (2006) Involvement of the CXCL12/CXCR4 pathway in the recovery of skin following burns. *J. Invest. Dermatol.* **126,** 468–476

19. Cashen, A. F. (2009) Plerixafor hydrochloride: a novel agent for the mobilization of peripheral blood stem cells. *Drugs Today* **45,** 497–505

20. Liang, Z., Zhan, W., Zhu, A., Yoon, Y., Lin, S., Sasaki, M., Klapproth, J. M., Yang, H., Grossniklaus, H. E., Xu, J., Rojas, M., Voll, R. J., Goodman, M. M., Arrendale, R. F., Liu, J., *et al.* (2012) Development of a unique small molecule modulator of CXCR4. *PLoS ONE* **7,** e34038

21. Tamamura, H., Hori, A., Kanzaki, N., Hiramatsu, K., Mizumoto, M., Nakashima, H., Yamamoto, N., Otaka, A., and Fujii, N. (2003) T140 analogs as CXCR4 antagonists identified as anti-metastatic agents in the treatment of breast cancer. *FEBS Lett.* **550,** 79–83

22. Kuhne, M. R., Mulvey, T., Belanger, B., Chen, S., Pan, C., Chong, C., Cao, F., Niekro, W., Kempe, T., Henning, K. A., Cohen, L. J., Korman, A. J., and Cardarelli, P. M. (2013) BMS-936564/MDX-1338: a fully human anti-CXCR4 antibody induces apoptosis *in vitro* and shows antitumor activity *in vivo* in hematologic malignancies. *Clin. Cancer Res.* **19,** 357–366

23. Peng, L., Damschroder, M. M., Cook, K. E., Wu, H., and Dall'Acqua, W. F. (2016) Molecular basis for the antagonistic activity of an anti-CXCR4 antibody. *MAbs* **8,** 163–175

24. Weitzenfeld, P., and Ben-Baruch, A. (2014) The chemokine system, and its CCR5 and CXCR4 receptors, as potential targets for personalized therapy in cancer. *Cancer Lett.* **352,** 36–53

25. Coia, G., Hudson, P. J., and Lilley, G. G. (1996) Construction of recombinant extended single-chain antibody peptide conjugates for use in the diagnosis of HIV-1 and HIV-2. *J. Immunol. Methods* **192,** 13–23

26. Minsky, A., Summers, R. G., and Knowles, J. R. (1986) Secretion of β-lactamase into the periplasm of *Escherichia coli*: evidence for a distinct release step associated with a conformational change. *Proc. Natl. Acad. Sci. U.S.A.* **83,** 4180–4184

27. Hosse, R. J., Tay, L., Hattarki, M. K., Pontes-Braz, L., Pearce, L. A., Nuttall, S. D., and Dolezal, O. (2009) Kinetic screening of antibody-Im7 conjugates by capture on a colicin E7 DNase domain using optical biosensors. *Anal. Biochem.* **385,** 346–357

28. Coley, A. M., Campanale, N. V., Casey, J. L., Hodder, A. N., Crewther, P. E., Anders, R. F., Tilley, L. M., and Foley, M. (2001) Rapid and precise epitope mapping of monoclonal antibodies against *Plasmodium falciparum* AMA1 by combined phage display of fragments and random peptides. *Protein Eng.* **14,** 691–698

29. Kabsch, W. (2010) XDS. *Acta Crystallogr. D Biol. Crystallogr.* **66,** 125–132

30. Storoni, L. C., McCoy, A. J., and Read, R. J. (2004) Likelihood-enhanced fast rotation functions. *Acta Crystallogr. D Biol. Crystallogr.* **60,** 432–438

31. Emsley, P., and Cowtan, K. (2004) Coot: model-building tools for molecular graphics. *Acta Crystallogr. D Biol. Crystallogr.* **60,** 2126–2132

32. Adams, P. D., Afonine, P. V., Bunkóczi, G., Chen, V. B., Davis, I. W., Echols, N., Headd, J. J., Hung, L. W., Kapral, G. J., Grosse-Kunstleve, R. W., McCoy, A. J., Moriarty, N. W., Oeffner, R., Read, R. J., Richardson, D. C., *et al.* (2010) PHENIX: a comprehensive Python-based system for macromolecular structure solution. *Acta Crystallogr. D Biol. Crystallogr.* **66,** 213–221

33. Morin, A., Eisenbraun, B., Key, J., Sanschagrin, P. C., Timony, M. A., Ottaviano, M., and Sliz, P. (2013) Collaboration gets the most out of software. *eLife* **2,** e01456

34. Simmons, D. P., Streltsov, V. A., Dolezal, O., Hudson, P. J., Coley, A. M., Foley, M., Proll, D. F., and Nuttall, S. D. (2008) Shark IgNAR antibody mimotopes target a murine immunoglobulin through extended CDR3 loop structures. *Proteins* **71,** 119–130

35. Kunkel, T. A. (1985) Rapid and efficient site-specific mutagenesis without phenotypic selection. *Proc. Natl. Acad. Sci. U.S.A.* **82,** 488–492

36. Perugini, M. A., Schuck, P., and Howlett, G. J. (2000) Self-association of human apolipoprotein E3 and E4 in the presence and absence of phospholipid. *J. Biol. Chem.* **275,** 36758–36765

37. Hor, L., Peverelli, M. G., Perugini, M. A., and Hutton, C. A. (2013) A new robust kinetic assay for DAP epimerase activity. *Biochimie* **95,** 1949–1953

38. Laue, T. M., Shah, B. D., Ridgeway, T. M., and Pelletier, S. L. (1992) in *Analytical Ultracentrifugation in Biochemistry and Polymer Science* (Harding, S. E., Rowe, A. J., and Horton, J. C., eds) pp. 90–125, The Royal Society of Chemistry, Cambridge, UK

39. Schuck, P. (2000) Size-distribution analysis of macromolecules by sedimentation velocity ultracentrifugation and Lamm equation modeling. *Biophys. J.* **78,** 1606–1619

40. See, H. B., Seeber, R. M., Kocan, M., Eidne, K. A., and Pfleger, K. D. (2011) Application of G protein-coupled receptor-heteromer identification technology to monitor β-arrestin recruitment to G protein-coupled receptor heteromers. *Assay Drug Dev. Technol.* **9,** 21–30

41. Roche, M., Salimi, H., Duncan, R., Wilkinson, B. L., Chikere, K., Moore, M. S., Webb, N. E., Zappi, H., Sterjovski, J., Flynn, J. K., Ellett, A., Gray, L. R., Lee, B., Jubb, B., Westby, M., *et al.* (2013) A common mechanism of clinical HIV-1 resistance to the CCR5 antagonist maraviroc despite divergent resistance levels and lack of common gp120 resistance mutations. *Retrovirology* **10,** 43

42. Nilsson, S. K., Johnston, H. M., Whitty, G. A., Williams, B., Webb, R. J., Denhardt, D. T., Bertoncello, I., Bendall, L. J., Simmons, P. J., and Haylock, D. N. (2005) Osteopontin, a key component of the hematopoietic stem cell niche and regulator of primitive hematopoietic progenitor cells. *Blood* **106,** 1232–1239

43. Grassinger, J., Haylock, D. N., Storan, M. J., Haines, G. O., Williams, B., Whitty, G. A., Vinson, A. R., Be, C. L., Li, S., Sørensen, E. S., Tam, P. P., Denhardt, D. T., Sheppard, D., Choong, P. F., and Nilsson, S. K. (2009) Thrombin-cleaved osteopontin regulates hemopoietic stem and progenitor cell functions through interactions with α9β1 and α4β1 integrins. *Blood* **114,** 49–59

44. Haylock, D. N., Williams, B., Johnston, H. M., Liu, M. C., Rutherford, K. E., Whitty, G. A., Simmons, P. J., Bertoncello, I., and Nilsson, S. K. (2007) Hemopoietic stem cells with higher hemopoietic potential reside at the bone marrow endosteum. *Stem Cells* **25,** 1062–1069

45. Cao, B., Zhang, Z., Grassinger, J., Williams, B., Heazlewood, C. K., Churches, Q. I., James, S. A., Li, S., Papayannopoulou, T., and Nilsson, S. K. (2016) Therapeutic targeting and rapid mobilization of endosteal HSC using a small molecule integrin antagonist. *Nat. Commun.* **7,** 11007

46. Stanfield, R. L., Dooley, H., Flajnik, M. F., and Wilson, I. A. (2004) Crystal structure of a shark single-domain antibody V region in complex with lysozyme. *Science* **305,** 1770–1773

47. Qin, L., Kufareva, I., Holden, L. G., Wang, C., Zheng, Y., Zhao, C., Fenalti, G., Wu, H., Han, G. W., Cherezov, V., Abagyan, R., Stevens, R. C., and Handel, T. M. (2015) Structural biology. Crystal structure of the chemokine receptor CXCR4 in complex with a viral chemokine. *Science* **347,** 1117–1122

48. Kofuku, Y., Yoshiura, C., Ueda, T., Terasawa, H., Hirai, T., Tominaga, S., Hirose, M., Maeda, Y., Takahashi, H., Terashima, Y., Matsushima, K., and Shimada, I. (2009) Structural basis of the interaction between chemokine stromal cell-derived factor-1/CXCL12 and its G-protein-coupled receptor CXCR4. *J. Biol. Chem.* **284,** 35240–35250

49. Kenakin, T. (2011) Functional selectivity and biased receptor signaling. *J. Pharmacol. Exp. Ther.* **336,** 296–302

50. Steen, A., Larsen, O., Thiele, S., and Rosenkilde, M. M. (2014) Biased and G protein-independent signaling of chemokine receptors. *Front. Immunol.* **5,** 277

51. Fricker, S. P., Anastassov, V., Cox, J., Darkes, M. C., Grujic, O., Idzan, S. R., Labrecque, J., Lau, G., Mosi, R. M., Nelson, K. L., Qin, L., Santucci, Z., and Wong, R. S. (2006) Characterization of the molecular pharmacology of AMD3100: a specific antagonist of the G-protein coupled chemokine receptor, CXCR4. *Biochem. Pharmacol.* **72,** 588–596

52. De Clercq, E., Yamamoto, N., Pauwels, R., Balzarini, J., Witvrouw, M., De Vreese, K., Debyser, Z., Rosenwirth, B., Peichl, P., and Datema, R. (1994) Highly potent and selective inhibition of human immunodeficiency virus by the bicyclam derivative JM3100. *Antimicrob. Agents Chemother.* **38,** 668–674

53. Jakobsen, M. R., Cashin, K., Roche, M., Sterjovski, J., Ellett, A., Borm, K., Flynn, J., Erikstrup, C., Gouillou, M., Gray, L. R., Saksena, N. K., Wang, B., Purcell, D. F., Kallestrup, P., Zinyama-Gutsire, R., *et al.* (2013) Longitudinal analysis of CCR5 and CXCR4 usage in a cohort of antiretroviral therapy-naive subjects with progressive HIV-1 subtype C infection. *PLoS ONE* **8,** e65950

54. Bogan, A. A., and Thorn, K. S. (1998) Anatomy of hot spots in protein interfaces. *J. Mol. Biol.* **280,** 1–9

55. Lo Conte, L., Chothia, C., and Janin, J. (1999) The atomic structure of protein-protein recognition sites. *J. Mol. Biol.* **285,** 2177–2198

56. Rosenkilde, M. M., Gerlach, L. O., Jakobsen, J. S., Skerlj, R. T., Bridger, G. J., and Schwartz, T. W. (2004) Molecular mechanism of AMD3100 antagonism in the CXCR4 receptor: transfer of binding site to the CXCR3 receptor. *J. Biol. Chem.* **279,** 3033–3041

57. Carnec, X., Quan, L., Olson, W. C., Hazan, U., and Dragic, T. (2005) Anti-CXCR4 monoclonal antibodies recognizing overlapping epitopes differ significantly in their ability to inhibit entry of human immunodeficiency virus type 1. *J. Virol.* **79,** 1930–1933

58. Duarte, D. B., Vasko, M. R., and Fehrenbacher, J. C. (2012) Models of inflammation: carrageenan air pouch. *Curr. Protoc. Pharmacol.* 10.1002/0471141755.ph0506s56

59. Liles, W. C., Broxmeyer, H. E., Rodger, E., Wood, B., Hübel, K., Cooper, S., Hangoc, G., Bridger, G. J., Henson, G. W., Calandra, G., and Dale, D. C. (2003) Mobilization of hematopoietic progenitor cells in healthy volunteers by AMD3100, a CXCR4 antagonist. *Blood* **102,** 2728–2730

60. Broxmeyer, H. E., Orschell, C. M., Clapp, D. W., Hangoc, G., Cooper, S., Plett, P. A., Liles, W. C., Li, X., Graham-Evans, B., Campbell, T. B., Calandra, G., Bridger, G., Dale, D. C., and Srour, E. F. (2005) Rapid mobilization of murine and human hematopoietic stem and progenitor cells with AMD3100, a CXCR4 antagonist. *J. Exp. Med.* **201,** 1307–1318

61. Herr, D. R. (2012) Potential use of G protein-coupled receptor-blocking monoclonal antibodies as therapeutic agents for cancers. *Int. Rev. Cell Mol. Biol.* **297,** 45–81

62. Hutchings, C. J., Koglin, M., and Marshall, F. H. (2010) Therapeutic antibodies directed at G protein-coupled receptors. *MAbs* **2,** 594–606

63. Katritch, V., Cherezov, V., and Stevens, R. C. (2013) Structure-function of the G protein-coupled receptor superfamily. *Annu. Rev. Pharmacol. Toxicol.* **53,** 531–556

64. Burger, J. A., and Peled, A. (2009) CXCR4 antagonists: targeting the microenvironment in leukemia and other cancers. *Leukemia* **23,** 43–52

65. Hendrix, C. W., Collier, A. C., Lederman, M. M., Schols, D., Pollard, R. B., Brown, S., Jackson, J. B., Coombs, R. W., Glesby, M. J., Flexner, C. W., Bridger, G. J., Badel, K., MacFarland, R. T., Henson, G. W., Calandra, G., *et al.* (2004) Safety, pharmacokinetics, and antiviral activity of AMD3100, a selective CXCR4 receptor inhibitor, in HIV-1 infection. *J. Acquir. Immune Defic. Syndr.* **37,** 1253–1262

66. Roumen, L., Scholten, D. J., de Kruijf, P., de Esch, I. J., Leurs, R., and de Graaf, C. (2012) C(X)CR *in silico*: Computer-aided prediction of chemokine receptor-ligand interactions. *Drug Discov. Today Technol.* **9,** e281–291

67. Pfleger, K. D., Pawson, A. J., and Millar, R. P. (2008) Changes to gonadotropin-releasing hormone (GnRH) receptor extracellular loops differentially affect GnRH analog binding and activation: evidence for distinct ligand-stabilized receptor conformations. *Endocrinology* **149,** 3118–3129

68. Dar, A., Schajnovitz, A., Lapid, K., Kalinkovich, A., Itkin, T., Ludin, A., Kao, W. M., Battista, M., Tesio, M., Kollet, O., Cohen, N. N., Margalit, R., Buss, E. C., Baleux, F., Oishi, S., *et al.* (2011) Rapid mobilization of hematopoietic progenitors by AMD3100 and catecholamines is mediated by CXCR4-dependent SDF-1 release from bone marrow stromal cells. *Leukemia* **25,** 1286–1296

69. Petit, I., Szyper-Kravitz, M., Nagler, A., Lahav, M., Peled, A., Habler, L., Ponomaryov, T., Taichman, R. S., Arenzana-Seisdedos, F., Fujii, N., Sandbank, J., Zipori, D., and Lapidot, T. (2002) G-CSF induces stem cell mobilization by decreasing bone marrow SDF-1 and up-regulating CXCR4. *Nat. Immunol.* **3,** 687–694

70. Strieter, R. M., Keeley, E. C., Burdick, M. D., and Mehrad, B. (2009) The role of circulating mesenchymal progenitor cells, fibrocytes, in promoting pulmonary fibrosis. *Trans. Am. Clin. Climatol. Assoc.* **120,** 49–59

71. Phillips, R. J., Burdick, M. D., Hong, K., Lutz, M. A., Murray, L. A., Xue, Y. Y., Belperio, J. A., Keane, M. P., and Strieter, R. M. (2004) Circulating fibrocytes traffic to the lungs in response to CXCL12 and mediate fibrosis. *J. Clin. Invest.* **114,** 438–446

72. Shu, H. K., Yoon, Y., Hong, S., Xu, K., Gao, H., Hao, C., Torres-Gonzalez, E., Nayra, C., Rojas, M., and Shim, H. (2013) Inhibition of the CXCL12/CXCR4-axis as preventive therapy for radiation-induced pulmonary fibrosis. *PLoS ONE* **8,** e79768

73. Castaldo, C., Benicchi, T., Otrocka, M., Mori, E., Pilli, E., Ferruzzi, P., Valensin, S., Diamanti, D., Fecke, W., Varrone, M., and Porcari, V. (2014) CXCR4 antagonists: a screening strategy for identification of functionally selective ligands. *J. Biomol. Screen.* **19,** 859–869

74. Xu, J., Mora, A., Shim, H., Stecenko, A., Brigham, K. L., and Rojas, M. (2007) Role of the SDF-1/CXCR4 axis in the pathogenesis of lung injury and fibrosis. *Am. J. Respir. Cell Mol. Biol.* **37,** 291–299

75. Heym, R. G., Hornberger, W. B., Lakics, V., and Terstappen, G. C. (2015) Label-free detection of small-molecule binding to a GPCR in the membrane environment. *Biochim. Biophys. Acta* **1854,** 979–986